



NÚMERO: 436/2011

**UNIVERSIDADE ESTADUAL DE CAMPINAS
INSTITUTO DE GEOCIÊNCIAS
PÓS-GRADUAÇÃO EM GEOCIÊNCIAS
ÁREA DE GEOLOGIA E RECURSOS NATURAIS**

ANDRÉ LUIZ SILVA PESTILHO

Sistemática de isótopos estáveis aplicada à caracterização da evolução dos paleo-sistemas hidrotermais associados aos depósitos cupríferos Alvo Bacaba e Alvo Castanha, Província Mineral de Carajás, PA.

Dissertação de Mestrado apresentada ao Instituto de Geociências da UNICAMP para obtenção do título de Mestre em Geociências

ORIENTADORA: Profa. Dra Lena Virgínia Soares Monteiro

CO-ORIENTADOR: Prof. Dr. Roberto Perez Xavier

Este exemplar corresponde à versão final da dissertação defendida pelo aluno e orientado pela Profa. Dra.

Campinas - 2011

FICHA CATALOGRÁFICA ELABORADA POR
CÁSSIA RAQUEL DA SILVA – CRB8/5752 – BIBLIOTECA “CONRADO PASCHOALE” DO
INSTITUTO DE GEOCIÊNCIAS
UNICAMP

Unidade BECL
T/UNICAMP 1P439A
Cutter _____
V. _____ Ed. _____
Tombo BC 94682
Proc. 16-100-12
C _____ D x
Preço 111,00
Data 11/04/12
Cód. tit. 895822

P439s Pestilho, André Luiz Silva, 1985-
Sistemática de isótopos estáveis aplicada à
caracterização da evolução dos paleo-sistemas
hidrotermais associados aos depósitos cupríferos Alvo
Bacada e Alvo Castanha, Província Mineral do Carajás,
PA / André Luiz Silva Pestilho-- Campinas, SP.: [s.n.],
2011.

Orientador: Lena Virginia Soares Monteiro.
Coorientador: Roberto Perez Xavier.
Dissertação (mestrado) - Universidade Estadual de
Campinas, Instituto de Geociências.

1. Minas e recursos minerais – Carajás, Serra dos
(PA). 2. Cobre – Minas e mineração. 3. Isótopos
estáveis. I. Monteiro, Lena Virginia Soares, 1970- II.
Xavier, Roberto Perez, 1958- III. Universidade Estadual
de Campinas, Instituto de Geociências. IV. Título.

Informações para a Biblioteca Digital

Título em ingles: . Stable isotope systematic applied to characterization of the hydrothermal systems associated with the Alvo Bacaba and Alvo Castanha copper deposits, Carajás Mineral Province, PA.

Palavras-chaves em ingles:

Mines and mineral resources - Carajás Serra dos (PA)
Copper - Mines and Mining
Stable isotopes

Área de concentração: Geologia e Recursos Naturais

Titulação: Mestre em Geociências.

Banca examinadora:

Lena Virgínia Soares Monteiro (Presidente)
Elson Paiva de Oliveira
Jorge Silva Bittencourt

Data da defesa: 26-08-2011

Programa de Pós-graduação em Geociências



UNICAMP

UNIVERSIDADE ESTADUAL DE CAMPINAS
INSTITUTO DE GEOCIÊNCIAS
PÓS-GRADUAÇÃO EM GEOCIÊNCIAS NA
ÁREA DE GEOLOGIA E RECURSOS NATURAIS

AUTOR: André Luiz Silva Pestilho

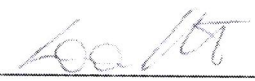
“Sistemática de isótopos estáveis aplicada à caracterização da evolução dos paleo-sistemas hidrotermais associados aos depósitos cupríferos Alvo Bacaba e Alvo Castanha, Província Mineral de Carajás, PA”

ORIENTADORA: Profa. Dra. Lena Virginia Soares Monteiro

CO-ORIENTADOR: Prof. Dr. Roberto Perez Xavier

Aprovada em: 26 / 08 / 2011

EXAMINADORES:

Profa. Dra. Lena Virginia Soares Monteiro  - Presidente

Prof. Dr. Elson Paiva de Oliveira 

Prof. Dr. Jorge Silva Bettencourt 

Campinas, 26 de agosto de 2011.

201207606

“A man who does not think for himself does not think at all.” –
Por Oscar Wilde, extraído do ensaio “The soul of man under Socialism”.

BIOGRAFIA

AGRADECIMENTOS

É realmente difícil lembrar-se de todas as pessoas que devemos agradecer quando chega o momento. Talvez apenas uma página ou duas numa dissertação seja algo tão pequeno, ou até mesmo menor, que um simples obrigado sincero dito em um corredor da universidade. Pois nem é possível saber se os agradecimentos serão lidos por quem somos gratos. Não obstante, agradecer aqui é a única oportunidade de exercer a liberdade, no único espaço em que o rigor técnico não oblitera a arte e priva os sentimentos.

A Professora Lena Virgínia Soares Monteiro sem dúvida é a pessoa a quem devo maior agradecimento durante esta etapa, não só por todos os ensinamentos e conselhos, e tudo que já tive a oportunidade de agradecer, mas também pela compreensão e por todo apoio em minhas decisões. Mais do que o conhecimento passado, a Lena, me ensinou muito sobre convivência e ética profissional, se houvessem mais professores esforçados como ela, sem dúvida ninguém se formaria com defasagem educacional.

Também agradeço especialmente ao Professor Roberto Perez Xavier pelo auxílio e pelas discussões em que me embasei para tirar minhas próprias conclusões sobre este trabalho.

Agradeço à minha mãe, Inez Silva Pestilho, por todo amor e pela fé em mim, durante toda provação, mesmo sem saber o significado do que e para que eu estava estudando isto.

Agradeço com todo meu amor, à Pamela Cardoso Vilela, que me trouxe muito amor e companheirismo durante todo este período de estudos, apoiando e ouvindo, sempre dedicada e carinhosa. Sempre vou lembrar aqueles finais de tarde, quando após um dia separando amostras de minerais ou escrevendo este texto, ela esteve presente, fazendo-me sorrir e animando-me.

Aos amigos, eu agradeço a todos, mas especialmente ao Rafael Rodrigues de Assis pela paciência e pelo companheirismo, especialmente durante os períodos de mudança de nossas vidas, eu desejo que ele tenha muito sucesso nessa vida. Um obrigado aos velhos amigos Gabriel Bueno Martins e ao Paulo Henrique Oliveira, pelos papos e desabafos de fins de semana. Obrigado também ao Leandro Rodrigues Magalhães de Marco pelas conversas e os cafés eventualmente acompanhados por profundas discussões.

Obrigado também a Karen Cristina Perles e a Ana Carolina Buzato Marchi pelas conversas e pelo contínuo apoio, mesmo depois que nossos caminhos se afastaram. Também agradeço a Evângela Patrícia Alves da Silva, que me apoiou principalmente em todas as mudanças que ocorreram em minha vida.

Agradeço àqueles que viabilizaram este estudo, como a Companhia VALE, que permitiu nossa entrada em suas minas, a coleta de testemunhos e o suporte necessário para a pesquisa. Em especial eu gostaria de agradecer ao Benevides Aires por todo o trabalho. Também agradeço a Carolina Penteado Moreto e ao Professor Caetano Juliani pelo apoio durante o reconhecimento geológico regional e a descrição dos testemunhos que foi realizada.

Agradeço também a FAPESP pela concessão da bolsa que viabilizou este projeto.

Finally, but still important, I would like to thank Professor Anthony Edward Fallick for his priceless contribution with all isotopic analyses. I feel very ashamed due to my own slowness in finishing this study. I really hope I have reached reasonable interpretations and conclusions about these data.

Sumário

INTRODUÇÃO	1
OBJETIVOS E JUSTIFICATIVAS	2
MÉTODOS DE ESTUDO	3
APRESENTAÇÃO DO ARTIGO	4
ANEXO 01	5
HYDROTHERMAL ALTERATION AND STABLE ISOTOPE STUDY OF ALVO BACABA AND ALVO CASTANHA COPPER DEPOSITS, CARAJÁS MINERAL PROVINCE, BRAZIL	5
ABSTRACT	5
1. INTRODUCTION	7
2. THE CARAJÁS MINERAL PROVINCE GEOLOGICAL SETTINGS	8
3. SAMPLING AND ANALYTICAL METHODS	14
4. ALVO BACABA AND ALVO CASTANHA GEOLOGICAL SETTING	16
5. CARBON, OXYGEN AND HYDROGEN STABLE ISOTOPES	33
6. SULFUR ISOTOPES	47
7. DISCUSSION	50
8. CONCLUSIONS	53
ACKNOWLEDGEMENTS	54
REFERENCES	55

ÍNDICE DE FIGURAS

FIGURE 1 – GEOLOGICAL MAP OF THE SOSSEGO MINE AREA, SHOWING THE LOCATION OF THE ALVO BACABA, ALVO CASTANHA AND ALVO JATOBÁ (MODIFIED FROM VALE; NOT PUBLISHED). ...	8
FIGURE 2 – REGIONAL MAP: 1 – CARAJÁS MINERAL PROVINCE AND ITS DIVISIONS: I.S.B. – ITACAÚNAS SHEAR BELT; R.M.G.G. – RIO MARIA GRANITE GREENSTONE TERRANME. 2 - A GEOLOGIC MAP OF THE CARAJÁS DOMAIN AND THE TRANSITION DOMAIN, SHOWING THE MAJOR ORE DEPOSITS (DOCEGEO 1988, CPRM 2004).	9
FIGURE 3 – FEATURES FROM ALVO BACABA HOST ROCKS. (A) MICROGRAPHIC TEXTURE IN THE SERRA DOURADA GRANITE. (B) SERRA DOURADA GRANITE AS IT OCCURS IN THE LESS HYDROTHERMALLY ALTERED AREAS SHOWING PRESERVED PHANERITIC TEXTURE. (C) BACABA TONALITE CUT BY VEINS OF QUARTZ AND SCAPOLITE. (D) BACABA TONALITE SHOWING VEINLETS OF TOURMALINE AND SCAPOLITE. (E) ALKALI FELDSPAR VEIN IN THE SERRA DOURADA GRANITE. (F) SERRA DOURADA GRANITE IN THIN SECTION, SHOWING PLAGIOCLASE PARTLY REPLACED BY POTASSIUM FELDSPAR AND SERICITE (TL, CP). ABBREVIATIONS: TL – TRANSMITTED LIGHT, CP – CROSSED POLARIZERS, KFS – ALKALI FELDSPAR, PL – PLAGIOCLASE, QTZ – QUARTZ, SER – SERICITE.	17
FIGURE 4 – FEATURES FROM THE ALVO CASTANHA HOST ROCKS. (A) ASPECT OF THE GABBRO AS IT APPEARS IN ALTERED DRILL CORE SAMPLES FROM THE ALVO CASTANHA DEPOSIT. (B) HYDROTHERMALLY ALTERED CASTANHA QUARTZ-FELDSPAR PORPHYRY AS IT OCCURS IN THE NEAREST AREAS FROM THE MAGNETITITE OREBODIES. (C) RELIC OF IGNEOUS TEXTURE IN GABBRO FROM ALVO CASTANHA (TL, CP). (D) ALBITE MEGACRYSTAL WITH CHESSBOARD TEXTURE IN THE CASTANHA FELDSPAR-QUARTZ PORPHYRY (TL, CP). (E) RELIC OF IGNEOUS TEXTURE IN GABBRO FROM ALVO BACABA (TL, CP). (F) EUHEDRAL QUARTZ MEGACRYSTAL INVOLVED BY HYDROTHERMAL BIOTITE IN THE CASTANHA FELDSPAR-QUARTZ PORPHYRY (TL, CP). ABBREVIATIONS: TL – TRANSMITTED LIGHT, CP – CROSSED POLARIZERS, KFS – ALKALI FELDSPAR, PL – PLAGIOCLASE, QTZ – QUARTZ, SER – SERICITE.	19
FIGURE 5 – ALVO BACABA AND ALVO CASTANHA PARAGENETIC EVOLUTION CHART (MODIFIED FROM AUGUSTO <i>ET AL.</i> 2008, AND PESTILHO AND MONTEIRO 2008).	20
FIGURE 6 – DRILL CORE SAMPLES FROM ALVO BACABA AND ALVO CASTANHA SHOWING HYDROTHERMAL ALTERATION FEATURES. ALL SAMPLES HAVE 2.5 CM HEIGHT. (A) ALBITE VEIN PARTIALLY REPLACED BY PERVASIVE POTASSIC ALTERATION ZONE WITH BIOTITE ASSOCIATED WITH DISSEMINATED SCAPOLITE CRYSTALS. POST POTASSIC ALTERATION QUARTZ VEIN ASSOCIATED WITH CHALCOPYRITE ARE ALSO DISPLAYED. (B) ALBITE ALTERATION REPLACED BY SCAPOLITE ALTERATION AND PERVASIVE POTASSIC ALTERATION WITH BIOTITE, RESPECTIVELY. (C) POTASSIC FELDSPAR ASSOCIATED WITH BIOTITE AND QUARTZ VEINS. (D) MAGNETITE AND ACTINOLITE OVERPRINTED BY COPPER MINERALIZATION (E) ASSOCIATION OF POTASSIC FELDSPAR, BIOTITE AND CALCITE. (F) POTASSIC FELDSPAR ASSOCIATED TO BIOTITE, SERICITE AND QUARTZ. ABV: AB – ALBITE, BT – BIOTITE, CAL – CALCITE, KFS – ALKALI FELDSPAR, CPY – CHALCOPYRITE, QTZ – QUARTZ, SER – SERICITE, SCP – SCAPOLITE.	25
FIGURE 8 – DRILL CORE SAMPLES FROM ALVO BACABA AND ALVO CASTANHA SHOWING HYDROTHERMAL ALTERATION FEATURES. ALL SAMPLES HAVE 2.5 CM HEIGHT. (A) CHLORITE VEINS CROSSCUT POTASSIC ALTERATION. CHLORITE SHOWS ASSOCIATION WITH SERICITE. (B) MAGNETITE CROSSCUT BY QUARTZ+BIOTITE VEIN SHOWING COMB TEXTURE. (C) PARTIALLY OVERPRINTED POTASSIC FELDSPAR AND BIOTITE BY SERICITE AND QUARTZ. (D) SERICITE	

REPLACING BIOTITE-RICH POTASSIC ALTERED ROCK. ABBREVIATIONS: TL – TRANSMITTED LIGHT, CP – CROSSED POLARIZERS, PP – PARALLEL POLARIZERS, AB – ALBITE, BT – BIOTITE, CAL – CALCITE, CHL – CHLORITE, HS – HASTINGSITE, KFS – ALKALI FELDSPAR, QTZ – QUARTZ, SER – SERICITE, SCP – SCAPOLITE, TUR – TOURMALINE.29

FIGURE 9 – HYDROTHERMAL ALTERATION ASSEMBLAGES FROM ALVO CASTANHA: (A) AND (B) SHOW SCAPOLITE PARTIALLY REPLACED BY BIOTITE FROM BOTH DEPOSITS. (C) TOURMALINE, BIOTITE, SCAPOLITE AND PYRITE ASSOCIATION (LT, CP). (D) MINERAL ASSOCIATION COMPOSED OF BIOTITE, TOURMALINE, QUARTZ AND CHLORITE (TL, PP). (E) CALCITE, ALKALI FELDSPAR, SERICITE AND HEMATITE WITHIN ALKALI FELDSPAR VEINS (TL, CP). (F) CALCITE VEIN WITH CHLORITE PSEUDOMORPHS (WITH BIOTITE HABIT), CHLORITE, HASTINGSITE AND SCAPOLITE INCLUSIONS (TL, CP). ABBREVIATIONS: TL – TRANSMITTED LIGHT, CP – CROSSED POLARIZERS, PP – PARALLEL POLARIZERS, AB – ALBITE, BT – BIOTITE, CAL – CALCITE, CHL – CHLORITE, HS – HASTINGSITE, KFS – ALKALI FELDSPAR, QTZ – QUARTZ, SER – SERICITE, SCP – SCAPOLITE, TUR – TOURMALINE.....29

FIGURE 10 – ORE MINERAL ASSOCIATION IN ALVO BACABA AND ALVO CASTANHA. ALL DRILL CORE SAMPLES HAVE 2.5 CM HEIGHT. ALL THIN SECTION IMAGES WERE TAKEN IN REFLECTED LIGHT WITH PARALLEL POLARIZERS. (A) AND (B) SHOW ALVO BACABA MINERALIZED BRECCIAS WITH MATRIX MAINLY COMPOSED OF CHALCOPYRITE ASSOCIATED WITH QUARTZ, BIOTITE AND SPECIALLY POTASSIC FELDSPAR CLASTS. (C) CHALCOPYRITE AND MAGNETITE PARTIALLY SUBSTITUTED BY HEMATITE. (D) BORNITE AND CHALCOPYRITE ASSOCIATION. (E) MAGNETITE WITH TABULAR HABIT (PROBABLY MUSKETOVITE) ASSOCIATED WITH CHALCOPYRITE. (F) MAGNETITE PARTIALLY REPLACED BY HEMATITE. (G) AND (H) SHOW MINERALIZED BRECCIAS WITH MATRIX MAINLY COMPOSED BY PYRRHOTITE, CHALCOPYRITE AND CALCITE WITH BIOTITE+QUARTZ+/-SCAPOLITE CLASTS. (I) PYRITE AND CHALCOPYRITE ASSOCIATION IN QUARTZ VEINS DISTAL IN RELATION TO THE MINERALIZED BRECCIA BODIES. (J) CHALCOPYRITE, PYRRHOTITE AND MAGNETITE ASSOCIATION, SHOWING PYRRHOTITE INSIDE OF MAGNETITE FRACTURES. (K) MINERALIZED BRECCIA SHOWING ASSOCIATION AMONG SPHALERITE, CHALCOPYRITE AND PYRRHOTITE. (L) PENTLANDITE FLAME TEXTURE INDICATED BY A DARK ARROW, IN PYRRHOTITE, ASSOCIATED TO CHALCOPYRITE IN ORE BRECCIAS. ABBREVIATIONS: AP – APATITE, BN – BORNITE, BT – BIOTITE, CAL – CALCITE, CPY – CHALCOPYRITE, HEM – HEMATITE, MT – MAGNETITE, PO – PYRRHOTITE, PN – PENTLANDITE, PY – PYRITE, QTZ – QUARTZ, SCP – SCAPOLITE.....33

FIGURE 11 – $\Delta^{18}\text{O}$ VERSUS ΔD PLOT FROM FLUID IN EQUILIBRIUM WITH DIFFERENT HYDROTHERMAL ALTERATION STAGES OF THE ALVO BACABA AND ALVO CASTANHA DEPOSITS, ACCORDING TO DATA FROM TABLE 3. VALUES FOR MAGMATIC WATERS, METAMORPHIC WATERS AND STANDARD MEAN OCEAN WATERS (SMOW) ARE FROM SHEPPARD (1986), FOR VOLCANIC VAPOURS ARE FROM GIGGENBACH (1992), AND FOR THE METEORIC WATER LINE (MWL) ARE FROM CRAIG (1967).42

FIGURE 12 – $\Delta^{18}\text{O}$ VERSUS $\Delta^{13}\text{C}$ GRAPH OF FLUID IN EQUILIBRIUM WITH CALCITE. IN THE ALVO BACABA, CI AND CII ASSOCIATIONS CORRESPOND TO THE SAMPLED CALCITE MINERAL ASSOCIATIONS (1) AND (2), WHEREAS CIII CORRESPONDS TO THE CALCITE ASSOCIATION (3). IN THE ALVO CASTANHA ALL SAMPLES CORRESPOND TO THE ASSOCIATION (4) WITH THE EXCEPTION OF THE ASSOCIATION MARKED WITH (*), WHICH CORRESPONDS TO THE ASSOCIATION (5).44

FIGURE 13 – OXYGEN ISOTOPIC COMPOSITION OF HYDROTHERMAL FLUIDS ASSOCIATED WITH DIFFERENT ALTERATION STAGES AND HYDROTHERMAL MINERALS FROM THE ALVO BACABA

AND ALVO CASTANHA DEPOSITS. MAGMATIC FLUID VALUES ARE FROM SHEPPARD (1986).
ABBREVIATIONS ACCORDING TO TABLE 5.....46

FIGURE 14 – $\Delta^{34}\text{S}$ VALUES FOR COPPER DEPOSITS (ALVO CASTANHA, ALVO BACABA, ALVO
VICONDE, ALVO BACURI AND PEDRA BRANCA) AND SMALL IRREGULAR MINES (*GARIMPOS*) IN
THE CARAJÁS MINERAL PROVINCE. NOTE: * – THIS STUDY; 1 – MONTEIRO *ET AL.* (2007); 2 –
TORRESI *ET AL.* (2009).....47

FIGURE 15 – SULFUR ISOTOPIC COMPOSITION OF SULFIDES FROM MAJOR IRON-OXIDE-COPPER
DEPOSITS AT THE CARAJÁS MINERAL PROVINCE (SOSSEGO, CRISTALINO, ALVO 118), MINOR
COPPER DEPOSITS (ALVO CASTANHA, ALVO BACABA, ALVO VICONDE, ALVO BACURI AND
PEDRA BRANCA), SMALL IRREGULAR MINES (*GARIMPOS*). NOTE: * – THIS STUDY; 1 –
MONTEIRO *ET AL.* (2007); 2 – TORRESI *ET AL.* (2009); 3 – RIBEIRO (2008).48

FIGURE 16 – ISOVALUE MAP FOR MAXIMUM $\Delta^{34}\text{S}_{\text{CDT}}$ VALUES FOR COPPER DEPOSITS ON THE
SURROUNDINGS OF THE SOSSEGO MINE. THE TREND SURFACE WAS OBTAINED BY ORDINARY
KRIGING AND THE VARIOGRAM WAS ADJUSTED TO THE SPHERICAL MODEL.49

ÍNDICE DE TABELAS

TABLE 1 – OXYGEN AND HYDROGEN ISOTOPIC DATA FOR SILICATES AND OXIDES.	34
TABLE 2 – OXYGEN AND CARBON ISOTOPIC DATA AQUIRED FOR CALCITE SAMPLES.	36
TABLE 3 – SULFUR ISOTOPIC DATA.....	37
TABLE 4 – ESTIMATED TEMPERATURE FROM MINERAL PAIRS IN ISOTOPIC EQUILIBRIUM FROM THE ALVO BACABA AND ALVO CASTANHA DEPOSITS. ABBREVIATIONS: ACT – ACTINOLITE, BT – BIOTITE, CC – CALCITE, QTZ – QUARTZ, MT – MAGNETITE.....	39
TABLE 5 – ESTIMATES OF FLUID ISOTOPIC COMPOSITIONS BASED ON CALCULATED TEMPERATURES FOR DIFFERENT ALTERATION STAGES OF THE ALVO BACABA AND CASTANHA DEPOSITS. NOTE: A – ESTIMATES DO NOT CONSIDER ANALYTICAL ERROR AND DEVIATION FROM THESE VALUES DO NOT REPRESENT ERROR. B – V-SMOW STANDARD. C – PDB STANDARD.....	40
TABLE 6 – HYDRATED MINERAL ISOTOPIC COMPOSITION AND ASSOCIATED ERROR WITH CALCULATIONS BASED ON PALEOTHERMOMETRIC TEMPERATURES AND ESTIMATED TEMPERATURES. NOTE: A – ALMOST ALL VALUES WERE CALCULATED USING ISOTOPIC GEOTHERMOMETRY, AND IT CONSIDERS ANALYTICAL ERROR OF 0.2‰ FOR OXYGEN AND 2‰ FOR HYDROGEN. VALUES WITH * WERE CALCULATED USING EMPIRICAL ESTIMATES OF TEMPERATURE, EVEN THOUGH IT CONSIDERS ANALYTICAL ERROR. B – VERSUS V-SMOW.	41



UNIVERSIDADE ESTADUAL DE CAMPINAS
INSTITUTO DE GEOCIÊNCIAS
PÓS-GRADUAÇÃO EM GEOCIÊNCIAS
ÁREA DE GEOLOGIA E RECURSOS NATURAIS

RESUMO

DISSERTAÇÃO DE MESTRADO

ANDRÉ LUIZ SILVA PESTILHO

Localizados na porção norte da Província Mineral de Carajás, a uma distância de cerca de 8 km do depósito de óxido de ferro-cobre-ouro de Sossego, estão os depósitos de cobre Alvo Bacaba e Alvo Castanha. Esses depósitos encontram-se ao longo de uma zona de cisalhamento regional de cerca de 60 km de extensão, no limite entre o Supergrupo Itacaúnas e seu embasamento representados principalmente pelos migmatitos do complexo Xingu.

O Alvo Bacaba é hospedado pelo granito Serra Dourada e pelo tonalito Bacaba, enquanto o Alvo Castanha é Ambos os depósitos exibem amplas zonas de alteração hidrotermal que compreendem quase que respectivamente a albitização, a escapolitização, a formação de óxidos de ferro, a alteração sódico-cálcica, a alteração potássica, a formação de turmalina, a sericitização, a cloritização, a epidotização e a carbonatização, embora estes depósitos mostrem diferenças, como a alteração sódico-cálcica que apesar de ser bem desenvolvida no Alvo Castanha, é quase inexistente no Alvo Bacaba, onde apenas ocorre como alteração nos gabros. Também o Alvo Bacaba possui uma associação de minerais distintas, composta por calcopirita±pirita±bornita, enquanto o Alvo Castanha exhibe a associação calcopirita±pirrotita±pirita.

Informações sobre evolução paragenética e dados de isótopos estáveis indicam que os depósitos Alvo Bacaba e Alvo Castanha evoluíram durante progressivo resfriamento. Entretanto, esta redução com relação à evolução paragenética foi maior no Alvo Bacaba do que no Alvo Castanha, e a fugacidade de oxigênio foi mantida alta no Alvo Bacaba. A temperatura de deposição do minério estimada para o Alvo Bacaba pode ter ocorrido entre 220 °C e 410 °C, enquanto no Alvo Castanha esta teria ocorrido entre 350 °C e 420 °C. A evolução isotópica do Alvo Bacaba é similar àquela caracterizada para o depósito de Sossego, com uma redução acentuada da temperatura acompanhada por um decréscimo no valor de $\delta^{18}\text{O}$ e acréscimo no valor de δD e evidências de misturas de fluido juvenil e de fonte não magmática. Já para o Alvo Castanha, as composições isotópicas dos fluidos hidrotermais indicam a predominância de uma fonte magmática.

Estas características e similaridades com aquelas de Sossego podem apontar para uma contribuição de águas magmáticas e oceânicas no sistema hidrotermal que originou todos estes depósitos.



UNIVERSIDADE ESTADUAL DE CAMPINAS
INSTITUTO DE GEOCIÊNCIAS
PÓS-GRADUAÇÃO EM GEOCIÊNCIAS
ÁREA DE GEOLOGIA E RECURSOS NATURAIS

ABSTRACT

DISSERTAÇÃO DE MESTRADO

ANDRÉ LUIZ SILVA PESTILHO

The Alvo Bacaba and Alvo Castanha copper deposits are located at the northern part of the Carajás Mineral Province, at a distant radius of about 8 km from the Sossego iron oxide-copper-gold deposit. These deposits occur along a regional shear zone 60 km wide, in the limit between the Itacaiúnas Supergroup and its basement represented mainly by migmatites of the Xingu Complex.

Both deposits exhibits widespread hydrothermal alteration zones comprising albitization, scapolitization, iron oxide formation, sodic-calcic alteration, potassic alteration, tourmaline formation, sericitization, epidotization and carbonatization, although these two deposits show differences like sodic-calcic alteration, which is well developed in Alvo Castanha, but it is almost inexistant in Alvo Bacaba, being present only in its altered gabbros. Also the Alvo Bacaba shows ore minerals association essentially composed by chalcopyrite±pyrite±bornite while the Alvo Castanha shows the association of chalcopyrite±pyrrhotite±pyrite.

Paragenesis and stable isotope data indicate that the Alvo Bacaba and Alvo Castanha deposits have evolved with temperature decrease. However, the temperature drop in relation to the hydrothermal alteration succession was greater in Alvo Bacaba than the Alvo Castanha, and the oxygen fugacity was kept higher at Alvo Bacaba. The estimated temperature for ore deposition in the Alvo Bacaba was between 220 °C and 410 °C, while the Alvo Castanha it would have occurred between 350 °C and 420 °C. The isotopic evolution of the Alvo Bacaba is similar to that characterized for the Sossego deposit, with a steep temperature reduction accompanied by decrease of $\delta^{18}\text{O}$ and increase of δD values and fluid mixing evidences. In the Alvo Castanha, isotopic compositions of the hydrothermal fluids indicate predominance of magmatic sources.

These characteristics and its similarities with those of the Sossego deposit could point to a contribution of magmatic and ocean waters in the hydrothermal system that originated all deposits.

INTRODUÇÃO

Este estudo apresenta a síntese dos resultados e conclusões do projeto de Mestrado intitulado “**Sistemática de isótopos estáveis aplicada à caracterização da evolução dos paleo-sistemas hidrotermais associados aos depósitos cupríferos Alvo Bacaba e Alvo Castanha, Província Mineral de Carajás, PA**”, apresentados na forma de um artigo a ser submetido a periódico especializado no escopo deste trabalho.

A Província Mineral de Carajás hospeda importantes depósitos cupro-auríferos localizados ao longo de uma zona de cisalhamento regional de direção WNW–ESE com cerca de 60 km, que define o contato sul entre o Supergrupo Itacaiúnas, metavulcano-sedimentar, e o embasamento, representado por gnaisses tonalíticos e trondhjemíticos e migmatitos do Complexo Xingu (DOCEGEO 1988).

Estes depósitos, considerados semelhantes aos depósitos de óxido de Fe-Cu-Au (*iron oxide-copper-gold deposits* ou IOCG como definido por Hitzman *et al.* 1992, 2000) se destacam pelo tamanho das reservas e teores, como os depósitos Salobo (com reservas de 789 Mt com 0,96% de Cu e 0,52 g/t de Au; Lindenmayer 1990), Igarapé Bahia-Alemão (219 Mt com 1,4% de Cu e 0,86 g/t de Au; Tavaza 1999, Tallarico *et al.* 2000, 2005), Sossego (355 Mt com 1,5 % de Cu e 0,28 g/t de Au; Cordeiro 1999, Lancaster e Olveira *et al.* 2000), Cristalino (500 Mt com 1,0% de Cu e 0,3 Au; Huhn *et al.* 1999) e Alvo 118 (70 Mt com 1,0% de Cu e 0,3 g/t de Au; Rigon *et al.* 2000). Além dessas jazidas, outros depósitos e ocorrências cupríferas ainda em avaliação, tais como Castanha, Bacaba, Jatobá e Visconde, são conhecidos.

Na Província Mineral de Carajás a relevância econômica destes depósitos os torna alvos importantes da pesquisa mineral, porém faltam subsídios de um modelo genético que, além de refletir as peculiaridades da evolução da província, possa auxiliar na distinção entre alvos econômicos e sub-econômicos, contribuindo para a elaboração de guias de prospecção mineral.

Os resultados obtidos neste estudo, que tem como tema os depósitos cupríferos Alvo Bacaba e Alvo Castanha, foram comparados aos de pesquisas similares realizadas para o depósito de Sossego (Carvalho 2005, Carvalho *et al.* 2009; Monteiro *et al.* 2007, 2008a, 2008b), o que permite um maior entendimento da evolução espacial e temporal do paleo-sistema hidrotermal que deu origem a estes depósitos.. Esse estudo integra pesquisas em andamento vinculadas à linha de pesquisa em Evolução Crustal e Metalogênese do Departamento de Geologia e Recursos

Naturais do Instituto de Geociências da UNICAMP, com ênfase na identificação de vetores associados a depósitos minerais. Os resultados apresentados fornecem subsídios para a proposição de modelos metalogenéticos e prospectivos alternativos para os depósitos IOCG da Província Mineral de Carajás, com base na compreensão de mecanismos que controlam as variações dos tipos de alteração e de minério nos depósitos IOCG dessa importante província metalogenética.

OBJETIVOS E JUSTIFICATIVAS

Com base na aplicação da sistemática de isótopos estáveis ao estudo dos halos de alteração hidrotermal e evolução dos paleo-sistemas hidrotermais associados aos depósitos de cobre Alvo Castanha e Alvo Bacaba, este projeto tem como objetivos:

- (1) Caracterizar a distribuição das zonas de alteração hidrotermal e suas relações com distintos níveis crustais e evolução temporal do sistema paleohidrotermal.
- (2) Identificar a natureza das fontes de fluidos, metais e enxofre, e a participação relativa das fontes, principalmente se múltiplas, na formação de diferentes depósitos de uma mesma província.
- (3) Identificar processos vinculados à evolução do(s) paleo-sistema(s) hidrotermal(is) e à deposição do minério.

A aplicação da geoquímica de isótopos estáveis na Província Mineral de Carajás possibilita considerações sobre a gênese dos depósitos sob o ponto de vista hidroquímico (Taylor 1987), baseado no reconhecimento de fluidos mineralizantes de diferentes origens e de evolução distintas, que incluem mistura de fluidos, processos de interação fluido-rocha e de magmas com a crosta superior. Como os estudos isotópicos dependem do conhecimento prévio da paragênese, características das inclusões fluidas, além do conhecimento necessário de paleogeografia, evolução estrutural e ambiente tectônico (Ohmoto & Rye 1979, Ohmoto 1986, Taylor 1987), é necessário para a aplicação dessa técnica o conhecimento dos alvos estudados. Por esse motivo, foram selecionados para esse estudos os depósitos Alvo Castanha e Alvo Bacaba, para os quais informações geológicas, incluindo estudos paragenéticos já são disponíveis (Monteiro *et al.* 2007, Pestilho & Monteiro 2008, Augusto *et al.* 2008) ou foram levantadas nos estudos realizados durante o desenvolvimento desse projeto de Mestrado.

MÉTODOS DE ESTUDO

(a) Revisão Bibliográfica

A revisão bibliográfica teve ênfase nos estudos sobre os depósitos de óxido de ferro–Cu–Au da Província Mineral de Carajás, sobre os modelos genéticos dos depósitos cupro–auríferos em contextos semelhantes em outras províncias metalogenéticas e em estudos sobre geoquímica isotópica aplicada aos estudos metalogenéticos.

(b) Levantamentos de Campo

Foi realizada uma etapa de campo no período de 14 a 25 de julho de 2009, quando foram realizadas atividades de reconhecimento do contexto geológico regional entre os dias 14 e 21, bem como a descrição sistemática e coleta de testemunhos do Alvo Castanha, entre os dias 22 e 25. Amostras previamente coletadas pela orientadora do estudo, tanto do Alvo Castanha como do Alvo Bacaba, também foram utilizadas nesse estudo. A amostragem total foi realizada em 6 furos de sondagem do Alvo Castanha e 16 do Alvo Bacaba.

(c) Petrografia em Luz Transmitida, Refletida e com uso de Microscopia Eletrônica de Varredura

Estudos petrográficos foram realizados visando à identificação de rochas hospedeiras das mineralizações, evolução paragenética associada aos diferentes tipos de alteração hidrotermal, relações texturais entre os minerais de minério e de ganga, relações entre paragêneses e microestruturas, sobreposições de feições tectônicas e de eventos hidrotermais.

(d) Geoquímica de Isótopos Estáveis

Análises de isótopos estáveis de carbono e oxigênio em calcita foram realizadas no NEGLABISE da Universidade Federal de Pernambuco, enquanto as análises de isótopos estáveis de enxofre, oxigênio e hidrogênio foram feitas no *Scottish Universities Environmental Research Centre* da Universidade de Glasgow, Escócia, em cooperação científica com o Prof. Dr. Anthony E. Fallick.

As análises de isótopos estáveis de oxigênio e hidrogênio foram efetuadas em fases mineralis representativas da evolução paragenética dos alvos investigados sendo que a análise conjunta destes isótopos permitiu, a partir do uso dos fatores de fracionamento isotópico mineral-

água determinados empírica ou teoricamente, juntamente com os valores de temperatura estimados para a mineralização a partir de pares minerais ou da microtermometria, a caracterização de variações nas composições isotópicas dos fluidos relacionadas à evolução temporal do sistema. Tais variações podem permitir o reconhecimento de processos, tais como a mistura entre diferentes fontes de fluidos, e complementação do entendimento da evolução paragenética do sistema por meio da correlação entre as temperaturas de equilíbrio em que se formaram os minerais hidrotermais.

Análises de isótopos de carbono e oxigênio em carbonatos e de enxofre em sulfetos foram realizadas objetivando a caracterização da história geoquímica da formação de carbonatos e sulfetos hidrotermais, visto que as composições isotópicas de $\delta^{13}\text{C}$ e $\delta^{34}\text{S}$ são fortemente controladas pelo estágio de oxidação, temperatura, pH e $P_{\text{H}_2\text{O}}$, com importantes implicações no reconhecimento de mecanismos de deposição do minério. Estas análises são indicativas da origem do enxofre e do carbono nos sistemas estudados, a partir do estabelecimento do balanço de massas entre espécies oxidadas e reduzidas desses elementos.

APRESENTAÇÃO DO ARTIGO

Os resultados obtidos são apresentados na forma de artigo científico (Anexo 01) intitulado *Hydrothermal Alteration and Stable Isotopes Study of the Alvo Castanha and Alvo Bacaba Copper Deposits, Carajás Mineral Province, Brazil* que será submetido ao periódico *Ore Geology Reviews*.

ANEXO 01

HYDROTHERMAL ALTERATION AND STABLE ISOTOPE STUDY OF THE ALVO BACABA AND ALVO CASTANHA COPPER DEPOSITS, CARAJÁS MINERAL PROVINCE, BRAZIL

André Luiz Silva Pestilho¹, Lena Virgínia Soares Monteiro¹, Anthony Edward Fallick², Roberto Perez Xavier¹, Carlos Roberto de Souza Filho¹

¹ *Institute of Geosciences, P.O. Box 6152, University of Campinas – UNICAMP, 13083-970, Campinas, SP, Brazil*

² *Scottish Universities Environmental Research Centre, East Kilbride, Glasgow, G75 0QU, Scotland, United Kingdom*

ABSTRACT

The Alvo Bacaba and Alvo Castanha copper deposits are located at the northern part of the Carajás Mineral Province, at a distant radius of about 8 km from the Sossego iron oxide-copper-gold deposit. These deposits occur along a regional shear zone 60 km wide, in the limit between the Itacaiúnas Supergroup and its basement represented mainly by migmatites of the Xingu Complex. Both deposits exhibit widespread hydrothermal alteration zones comprising albitization, scapolitization, iron oxide formation, sodic-calcic alteration, potassic alteration, tourmaline formation, sericitization, epidotization and carbonatization although these two deposits show differences like sodic-calcic alteration, which is well developed in Alvo Castanha, but it is almost inexistant in Alvo Bacaba, being present only in its altered gabbros. Also the Alvo Bacaba shows ore minerals association essentially composed of chalcopyrite±pyrite±bornite while the Alvo Castanha shows the association of chalcopyrite±pyrrhotite±pyrite. Paragenesis and stable isotope data indicate that the Alvo Bacaba and Alvo Castanha deposits have evolved with temperature decrease. However, the temperature drop in relation to the hydrothermal alteration succession was greater in Alvo Bacaba than the Alvo Castanha, and the oxygen fugacity was kept higher at Alvo Bacaba. The estimated temperature for ore deposition in the Alvo Bacaba was between 220 °C and 410 °C, while for the Alvo Castanha it was between 350 °C and 420 °C. The isotopic evolution of the Alvo Bacaba is similar to that characterized for the Sossego deposit, with a steep

temperature reduction accompanied by decrease of $\delta^{18}\text{O}$ and increase of δD values and fluid mixing.

In the Alvo Castanha, isotopic compositions of the hydrothermal fluids indicate predominance of magmatic sources. These characteristics and its similarities with those of the Sossego deposit could point to a contribution of magmatic and ocean waters in the hydrothermal system that originated all deposits.

1. INTRODUCTION

Located at the southeastern margin of the Amazon Craton, northern Brazil, the Carajás Mineral Province is one of the largest known polymetallic mineral provinces in the world. It hosts a series of large-tonnage world class iron oxide-copper-gold deposits (IOCG; Hitzman 1992, Hitzman *et al.* 2000), as example of Salobo (789 Mt at 0.96 wt.% Cu, 0.52 g/t Au, 55 g/t Ag; Souza and Vieira 2000), Cristalino (500 Mt at 1.0 wt.% Cu; 0.3 g/t Au, Huhn *et al.* 1999), Sossego (245 Mt at 1.1% Cu and 0.28 g/t Au; Lancaster *et al.* 2000), and Alvo 118 (170 Mt at 1.0 wt% Cu, 0.3 g/t Au; Rigon *et al.* 2000) deposits.

On the outskirts of the Sossego Mine, at a distant radius of about 8 km, there is a set of minor copper deposits (e.g. Alvo Bacaba, Alvo Bacuri, Alvo Castanha, Alvo Jatobá and Alvo Visconde) with a variable content of iron and/or gold, which are designated satellite targets due to their proximity and similarities to the Sossego orebodies. These similarities include geological features, such as structurally controlled mineralization style, types of hydrothermal alteration, metal content and similar light rare-earth-elements enrichment of the ore (Xavier *et al.* 2010). The study of these copper deposits is of paramount importance for the understanding of the genesis of the Sossego Mine and other IOCG deposits of the Carajás Mineral Province, which is still controversial, since geological information about them is relatively scarce, in special in wich concerns those minor deposits.

Among the satellite targets, the Alvo Bacaba and Alvo Castanha deposits (**Figure 1**) have been studied previously by Monteiro *et al.* (2007), Augusto *et al.* (2008) and Pestilho and Monteiro (2008). These deposits showed contrasting geological features in relation to the nature of the host rocks, hydrothermal alteration zones and metal enrichment, which are summarized here. This paper aims to present new data on the geological setting, paragenetic evolution, and stable isotopes constraints on the genesis of these deposits. This study may draw influences for undertanding the evolution of the hydrothermal system that originated these deposits and its relationship with the Sossego orebodies.

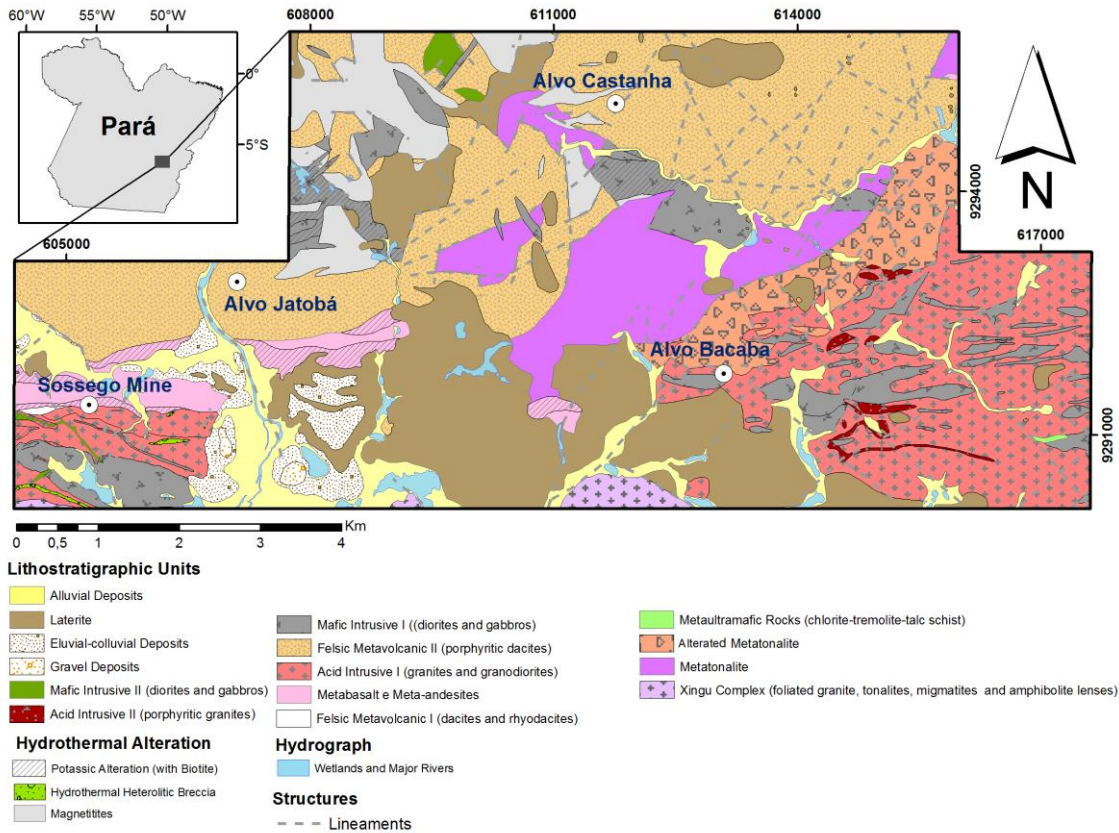


Figure 1 – Geological map of the Sossego Mine area, showing the location of the Alvo Bacaba, Alvo Castanha and Alvo Jatobá (modified from VALE; not published).

2. THE CARAJÁS MINERAL PROVINCE GEOLOGICAL SETTINGS

Comprising an Archean block within the Amazon Craton, the Carajás Mineral Province (CMP) is limited to the north by the Paleoproterozoic Maroni–Itacaiúnas belt, to the east by the Neoproterozoic Araguaia fold belt, to the west by Paleoproterozoic plutonic granitic rocks and related volcanic rocks, and to the south by the Phanerozoic sedimentary cover of the Parecis Basin (Tassinari and Macambira 2004). It is composed of two different tectonic domains: (I) the Rio Maria granite–greenstone terrane to the south (Huhn *et al.* 1988) and (II) the Carajás Domain to the north (Araújo *et al.* 1988). Both are limited by the Transition Domain (Gomes and Dall’Agnol 2007), also named Itacaiúnas Shear Zone Imbricated Domain (Araújo and Maia 1991, Araújo *et al.* 1994, Costa *et al.* 1995), whose limit is suggested by geophysical evidence to coincide with a regional EW trending discontinuity situated to the north of Sapucaia and south of Canaã dos Carajás towns (Oliveira *et al.* 2009).

2.1. THE CARAJÁS DOMAIN

The Carajás Domain (**Figure 2**) is composed of a basement represented by tonalitic to trondhjemitic gneiss and migmatite of the Xingu Complex (2974 ± 15 Ma U-Pb zircon, Machado *et al.* 1991), mafic to felsic orthogneisses of the Pium Complex (3002 ± 14 Ma U-Pb SHRIMP zircon, Pidgeon *et al.* 2000; 3050 ± 57 Ma Pb-Pb whole-rock, Rodrigues *et al.* 1992) and supracrustal sequences. Both basement units were affected by a coeval high-grade metamorphism that took place at ~2.85 Ga (2859 ± 2 Ma U-Pb zircon, Machado *et al.* 1991; 2859 ± 9 Ma U-Pb SHRIMP zircon, Pidgeon *et al.* 2000).

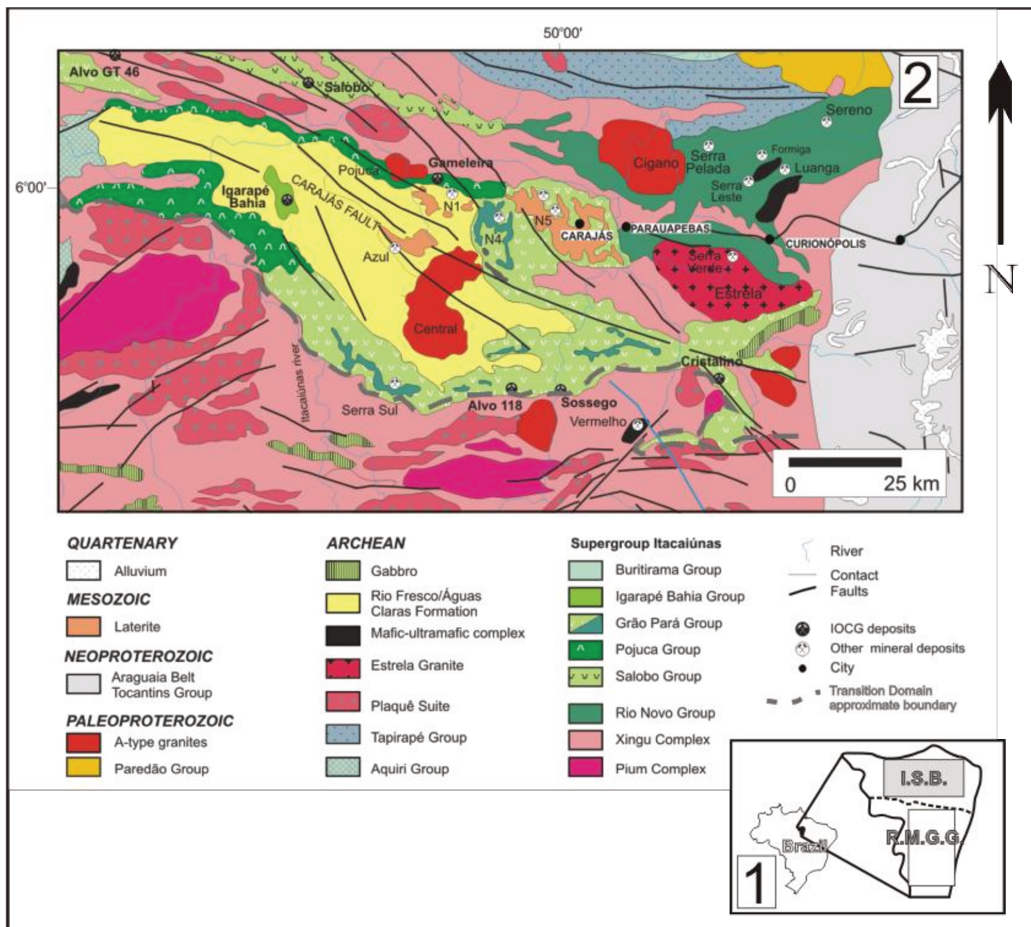


Figure 2 – Regional map: 1 – Carajás Mineral Province and its divisions: I.S.B. – Itacaúnas Shear Belt; R.M.G.G. – Rio Maria Granite Greenstone Terranme. 2 - A geologic map of the Carajás Domain and the Transition Domain, showing the major ore deposits (DOCEGEO 1988, CPRM 2004).

The supracrustal sequence that overlies the basement rocks is referred to the Archean Carajás Basin, and comprises the ~2.76 Ga metavolcanic-sedimentary Rio Novo Group (Hirata *et al.* 1982) and the 2.73 to 2.76 Ga Itacaiúnas Supergroup (Wirth *et al.* 1986, DOCEGEO 1988, Machado *et al.* 1991). Besides the younger sequences of shallow-water marine to fluvial clastic deposits designated as Rio Fresco Group (Beisiegel *et al.* 1973, DOCEGEO 1988), also called Águas Claras Formation (Araújo *et al.* 1988, Nogueira *et al.* 1995).

The Itacaiúnas Supergroup hosts known Carajás IOCG deposits (*eg.* Salobo, Igarapé Bahia/Alemão). It comprises the Igarapé Salobo (Wirth *et al.* 1986; 2761 ± 3 Ma U-Pb zircon, Machado *et al.* 1991), Igarapé Pojuca (DOCEGEO 1988; 2732 ± 3 Ma U-Pb zircon, Machado *et al.* 1991), Grão Pará (DOCEGEO 1988; 2759 ± 3 Ma U-Pb zircon, Machado *et al.*, 1991), and Igarapé Bahia groups (DOCEGEO 1988; 2747 ± 1 Ma Pb-Pb zircon, Galarza and Macambira 2002).

The Igarapé Salobo Group includes paragneisses, amphibolites, meta-arkoses and ironstone formation. The Igarapé Pojuca Group includes basic metavolcanic rocks, pelitic schists, amphibolites and iron formations metamorphosed at the greenschist to the amphibolite facies. The Grão Pará Group comprises metabasalts, felsic metavolcanic rocks and iron formation metamorphosed at lower-greenschist facies. Metavolcanic, metapyroclastic and ironstone rocks metamorphosed at greenschist facies are included in the Igarapé Bahia Group (DOCEGEO 1988).

Above the Itacaiúnas Supergroup, the Águas Claras Formation includes conglomerate, sandstone, locally manganese-rich dolomitic marble, talc-chlorite-rich rocks, carbonaceous siltstone and sericitic quartzites (Tallarico *et al.* 2000). This unit is constrained to be Archean by dating of detrital zircon in sandstones (2681 ± 5 Ma U-Pb SHRIMP, Trendall *et al.* 1998) and metagabbro sills (2645 ± 12 Ma U-Pb, Dias *et al.* 1996; 2708 ± 37 Ma U-Pb, Mougeot *et al.* 1996).

Distinct episodes of granitic magmatism have been identified in the Carajás Domain, including: (1) 2.76 to 2.74 Ga alkaline granites, comprising the Plaqué, Planalto, Estrela and Serra do Rabo suites (Huhn *et al.* 1999, Avelar *et al.* 1999, Barros *et al.* 2004, Sardinha *et al.* 2006); (2) 2.65 Ga dacitic to rhyolitic porphyry (2645 ± 9 Ma and 2654 ± 9 Ma; Pb-Pb SHRIMP zircon, Tallarico 2003), (3) 2.57 Ga peralkaline to meta-aluminous granites, characterized by the Old Salobo and Itacaiúnas granites (Machado *et al.* 1991, Souza *et al.* 1996); (4) 1.6 Ga alkali-rich leucogranite dyke with a U-Pb SHRIMP age of 1583 ± 7 Ma (Pimentel *et al.* 2003); (5) 1.88

Ga A-type alkaline to sub-alkaline granites, including the Central de Carajás, Young Salobo, Cigano, Pojuca, Breves granites (Machado *et al.* 1991, Dall'Agnoll *et al.* 1994, Lindenmayer and Teixeira 1999, Tallarico 2003); (6) Neoproterozoic (~600-550 Ma) Formiga Granite, which can represent the younger event of granite magmatism in the province (Grainger *et al.* 2008).

Different intrusive rocks also occur in this domain, including the ~2.75 Ga mafic-ultramafic intrusions of Luanga, Onça, Vermelho and Jacaré-Jacarezinho (Machado *et al.* 1991), the Borrachudo, Santa Inês and Complexo Lago Grande gabbros (Villas and Santos 2001), and late diabase dikes, whose radiometric ages are unknown.

The Carajás Domain complex structural settings have been attributed to the development of regional E-W trending steeply dipping fault zones that show evidence of several episodes of reactivation (Pinheiro and Holdsworth 1997, Holdsworth and Pinheiro 2000). According to these authors, the long time period of the tectonic evolution was given by several events: (1) 2.85-2.76 Ga – Sinistral transpression; (2) < 2.76 Ga – Pull-a-part basin formation with the Grão Pará Group deposition; (3) 2.7-2.6 Ga – Dextral transtension followed by the Cinzento and Carajás strike-slip shear zones development concomitant to the the Águas Claras Formation deposition and the island arc type magmatism, with plutons, mafic dykes and sills; (4) ~2.6 Ga – Tectonic basin inversion due to faults system reactivation; (5) 1.9-1.8 Ga – Structural extension or transtension, which favored the anorogenic granite plutons and mafic dyke swarm intrusion (Costa *et al.* 1995).

2.2. THE TRANSITION DOMAIN

The Transition Domain rocks host major IOCG deposits, such as the Sossego Mine, and several other copper deposits (e.g. Alvo Bacaba, Alvo Bacuri and Alvo Visconde). Feio *et al.* (2009) distinguished five magmatic associations based on geochemical evidence: (1) calc-alkaline leucogranites, (2) tonalitic calc-alkaline associations, (3) TTG-like trondhjemites, (4) Ti, Y and Zr-rich tonalitic-trondhjemitic associations (Gomes and Dall'agnol 2007), and (5) sub-alkaline A-type granites. Basic rocks, including variably deformed gabbro and amphibolites have been also identified (Gomes 2003).

Sardinha *et al.* (2004) reported Pb-Pb zircon ages for: (i) potassic leucomonzogranites with calc-alkaline affinity (2928 ± 1 Ma); (ii) sub-alkaline A-type biotite-hornblende granite (2734 ± 4

Ma), correlated to the Planalto granite, and (iii) trondhjemite of the tonalitic-trondhjemitic association (2765 ± 39 Ma).

The Neoproterozoic ages are comparable to those related to the extensive ca. 2.74 to 2.76 Ga alkaline magmatism recorded in the Carajás Domain, whereas the leucomonzogranites correlate to the Guaratã granite or the Caracol tonalite from the Rio Maria granite-greenstone terrane (Sardinha *et al.* 2004).

2.3. THE SOSSEGO DEPOSIT

The Sossego Mine, operated by VALE mining company since 2004, is classified as an iron oxide–copper–gold deposit. The Sossego deposit occurs along a regional east-southeast-striking shear zone that defines the southern contact between the Itacaiúnas Supergroup and its basement within the Transition Domain (Carvalho *et al.* 2005, Monteiro *et al.* 2008a, 2008b, Carvalho 2009, Xavier *et al.* 2009).

The Sossego deposit consists of two major orebody groups (Pista–Sequeirinho–Baiano and Sossego–Currál) with distinct alteration assemblages that are separated from each other by a major high angle fault. The deposit is hosted by granite, granophyric granite, gabbro, and felsic metavolcanic rocks (Monteiro *et al.* 2008a).

Sodic (albite-hematite association) and sodic-calcic hydrothermal alterations were characterized in both Sequeirinho and Baiano orebodies associated with massive magnetite-(apatite) bodies surrounded by actinolite-rich zones (actinolites), similar to other IOCG hydrothermal halos around the world (Monteiro *et al.* 2008a). These alterations are cut by spatially restricted zones of potassic (biotite and potassium feldspar) alteration that grade outwards to chlorite-rich assemblages (Monteiro *et al.* 2008a). The Pista orebody is hosted by mylonitized felsic metavolcanic rocks and exhibits a hydrothermal alteration stage characterized by biotite±hastingsite-turmaline–escapolite (Villas *et al.* 2005, Sousa 2007).

Nevertheless, the Sossego-Currál orebodies show more intensely developed potassic alteration, which is characterized by Cl-rich potassic feldspar and biotite that replace the granophyric granite. Chloritic alteration occurs mainly in the external halos associated with the hydrolytic alteration, represented by sericite-hematite-quartz association that is typical of very shallow sections in IOCG paleo-hydrothermal systems (Carvalho *et al.* 2005, Monteiro *et al.* 2008a, 2008b, Carvalho 2009).

Sulfide formation in both groups of orebodies is coeval to potassic alteration with potassium feldspar and a later assemblage of calcite–quartz–epidote–chlorite. The hydrothermal breccias from the Sequeirinho orebody have fragments of actinolites and actinolite, apatite and magnetite crystals within a chalcopyrite-rich matrix. The Sossego orebody breccias show angular to sub-angular fragments from the hydrothermally altered host rock involved by magnetite within a matrix composed of chalcopyrite, calcite, quartz, chlorite, actinolite, epidote and apatite with open-space filling textures (Carvalho *et al.* 2005, Monteiro *et al.* 2008a, 2008b, Carvalho 2009).

Pista–Sequeirinho–Baiano sulfides range from undeformed to deformed, but sulfides in the Sossego–Cural orebodies are undeformed (Monteiro *et al.* 2008a). The gold-copper mineralization formed during late stages in relation to the evolution of the hydrothermal system in brittle conditions. Ore minerals are represented by chalcopyrite associated with pyrite (up to 2.3 wt.% Co and 0.2 wt.% Ni), native gold (up to 14.9 wt.% Ag), siegenite, millerite, vaesite, Pd-melonite, and hessite (Monteiro *et al.* 2008b). Pyrrhotite and pyrite are minor ore minerals in the Sequeirinho orebody while pyrite is relatively abundant in the Sossego–Cural bodies (Monteiro *et al.* 2008a, 2008b, Carvalho 2009). Chalcopyrite Pb-Pb dating indicates age of breccia formation from Sequeirinho orebody at about 2608 ± 25 Ma (Neves *et al.* 2006, Villas *et al.* 2006).

Fluid inclusion studies from the Sossego deposit indicate that the chemical composition of the ore fluids is dominated by NaCl–CaCl₂–H₂O. Three different fluid types are related to the Cu-Au mineralization stages: (1) early mineralization stage: hypersaline and warm fluids (homogenization temperatures > 500 °C) composed of NaCl–CaCl₂–H₂O, with a NaCl/(NaCl + CaCl₂) ratio of 0.7; (2) main mineralization stage: low salinity fluids, with low homogenization temperatures (~ 150 °C) composed of NaCl–CaCl₂–H₂O, with a NaCl/(NaCl + CaCl₂) ratio of 0.3; (3) late mineralization stage: saline fluids, with low homogenization temperatures (< 250 °C) composed of NaCl–H₂O (Carvalho 2009).

The early sodic–calcic alteration stage of the Sequeirinho orebody was characterized by temperatures exceeding 500 °C and $\delta^{18}\text{O}_{\text{H}_2\text{O}}$ values for the hydrothermal fluid of $6.9 \pm 0.9\%$ (Monteiro *et al.* 2008a), which are consistent with fluid inclusion evidences of participation of early hot (>500 °C) brines (Carvalho 2009). Paragenetically later copper–gold mineralization displays markedly lower temperatures (< 300 °C) and was characterized by the introduction of $\delta^{18}\text{O}$ -depleted ($-1.8 \pm 3.4\%$) hydrothermal fluids (Monteiro *et al.* 2007, Monteiro *et al.* 2008a).

The δD_{H_2O} and $\delta^{18}O_{H_2O}$ values suggest that the fluids associated with the early sodic-calcic alteration assemblage were of magmatic or formational/metamorphic origin. Influx of $\delta^{18}O$ -depleted shallow-derived waters could be related to episodic fluid overpressure, resulting in dilution and cooling of the metalliferous fluid, causing deposition of metals transported as metal chloride complexes (Monteiro *et al.* 2007, Monteiro *et al.* 2008a, Carvalho 2009).

All Sossego orebodies show heavier sulfur ($\delta^{34}S=4.9\pm 2.4\%$) than expected for a mantle source (Monteiro *et al.* 2008a). According to Monteiro *et al.* (2008a) three possible sulfur sources were proposed for the Sossego paleo-hydrothermal system: (i) inorganically reduced Archean seawater sulfate/evaporate; (ii) inorganically reduced sulfate from continental evaporates; (iii) leached magmatic rocks or fluids from magmas that acquired most of their sulfur by assimilation of country rocks. However, the potential sulfur sources outlined above cannot be distinguished using the data set by Monteiro *et al.* (2008a). Calculated $\delta^{13}C_{CO_2}$ values for the Sossego–Curral and Sequeirinho mineralized breccias are $-4.3\pm 1.8\%$. This $\delta^{13}C_{CO_2}$ signature reflects values similar to those of the surrounding rocks.

3. SAMPLING AND ANALYTICAL METHODS

The methods included detailed sampling and description of drill cores, petrography, scanning electron microscope analysis (SEM) and carbon, oxygen, hydrogen, and sulfur stable isotope analysis. Petrography and scanning electron microscope analyses were performed at the Geosciences Institute, University of Campinas, Brazil. Electronic microscope analyses were performed in a SEM model LEO 430i equipped with an energy dispersive spectroscopy (EDS) and were used in the identification of heavy element-bearing minerals and mineral inclusions in polished thin sections.

Non-random mineral sampling for isotopic studies was carried out, looking for representative samples of each hydrothermal alteration stage. In an effort of characterize data representativity, error propagation analysis was performed (Bevington and Robinson 2002) over paleothermometric calculations and in D_{fluid} and $^{18}O_{fluid}$ values estimated from the isotopic composition of hydrated minerals, when a paragenetic mineral pair was found. For samples without a paragenetic pair, temperature was estimated by mineral stability fields available in the literature.

Mineral samples for stable isotope analysis were separated by crushing followed by mineral handpicking using a binocular magnifying glass. Carbon and oxygen isotopic compositions in calcite were determined at NEG-LABISE, Federal University of Pernambuco, Brazil, using the conventional digestion method (McCrea 1950). Powdered samples were reacted with H_3PO_4 at 25 °C to release the CO_2 . The $\delta^{13}\text{C}$ and $\delta^{18}\text{O}$ values were measured on cryogenically cleaned CO_2 (Craig 1957) in a triple collector SIRA II mass spectrometer. Borborema Skarn Calcite (BSC), calibrated in relation to international standards, was used as the reference gas and reproducibility of the measurements was better than $\pm 0.1\%$.

Sulfur, hydrogen and oxygen analyses were performed at the SUERC, University of Glasgow, Scotland. Sulfur isotopic analyses were based on the standard techniques of Robinson and Kusakabe (1975), using a Micromass SIRA-11 mass spectrometer for measuring the SO_2 gas. The ion beams monitored were m/z 66 and 64, with standard correction factors applied to raw $\delta^{34}\text{S}$ ratios (*eg.* Craig 1957). Long term reproducibility was better than $\pm 0.2\%$, based on repeated analyses of internal international and international standards. Hydrogen and oxygen analyses were performed using standard techniques.

Samples selected for hydrogen isotopic analysis had the amount of 30-50 mg of hydrogen extracted by heating samples under vacuum to release bound hydrogen, mostly as water vapor. Water was then converted to hydrogen by reaction with hot uranium. Samples were placed into platinum crucibles that had previously been heated under vacuum to 1500 °C for more than 3 hours, and the sample plus crucible was evacuated and degassed at 120 °C overnight prior to hydrogen extraction. The hydrogen produced was delivered to a mercury manometer by a Toepler pump and the yield determined by comparing the starting weight of mineral with the micromoles of gas produced. The extracted hydrogen was analyzed using a VG Micromass 602B mass spectrometer, with a working standard calibrated against international standards: NBS30 gives $\delta\text{D} = -65\%$. Estimated precision is $\pm 2\%$ for δD analyses.

Oxygen isotopic analyses of silicate minerals were made by extracting oxygen from samples of ~1 mg weight using a laser fluorination system based on that of Sharp (1990). Oxygen was released from the samples by heating them with a CO_2 laser whilst inside a ClF_3 -charged chamber. The oxygen was then converted to CO_2 and analyzed on a VG PRISM III mass spectrometer. In this technique each sample is reacted to completion so that the entire oxygen is collected, and as a result no laser correction factor is required. The analytical precision of the

laser fluorination technique is similar to the conventional fluorination technique at $\pm 0.2\%$, and gives good reproducibility regardless of sample grain size.

4. ALVO BACABA AND ALVO CASTANHA GEOLOGICAL SETTING

The Alvo Bacaba and Alvo Castanha deposits are still on evaluation by the VALE Company and estimation on tonnage and metal content were not available until this publication. Previous studies on these deposits (Augusto *et al.* 2008, Pestilho and Monteiro 2008, Moreto 2009, Moreto *et al.* 2011) and new data on host rocks, hydrothermal alteration and ore paragenetic relationships are presented below.

HOST ROCKS

In the Alvo Bacaba and Alvo Castanha area and its vicinities, strong mylonitization and hydrothermal alteration of the host rocks resulted in the almost complete obliteration of the original rock textures.

The Alvo Bacaba deposit, located within the Transition Domain, is hosted by the Serra Dourada Granite (2858 ± 30 Ma U-Pb zircon, Moreto *et al.* 2011), the Bacaba Tonalite ($3004 \pm 7,8$ Ma U-Pb zircon, Moreto *et al.* 2011) and gabbro bodies. The Serra Dourada Granite is light grayish pink with a predominant isotropic structure, coarse to medium equigranular texture with crystal sizes from 4 to 8 mm, which are mainly composed of quartz (~40%), white plagioclase (~30%), light red alkali feldspar (~20%), amphibole (~5%) and biotite (~5%). Accessory minerals include pyrite and magnetite. Micrographic textures and pegamatic facies (**Figure 3A**) of restrict occurrence have been recognized, as well as expressive disequilibrium textures related to hydrothermal alteration pervasive fronts. Veins and veinlets crosscut throughout the host rock (**Figure 3B, 3E**), sometimes showing open-space filling textures (*eg.* comb texture), especially close to the copper ore zones. Mylonitic foliation is typical of well developed pervasive hydrothermal alteration zones.

The Bacaba Tonalite (**Figures 3C, 3D**) is gray, isotropic to strongly foliated, medium-grained, has equigranular texture with crystal sizes from 1 to 8 mm and is composed of quartz (~40%), white plagioclase (~35%), amphibole (~10%), biotite (~10%) and light red alkali feldspar (~5%). Also the Bacaba Tonalite shows similar hydrothermal textures to those of the

Serra Dourada Granite, and it is difficult to distinguish each other in the intensely altered zones (**Figure 3F**).

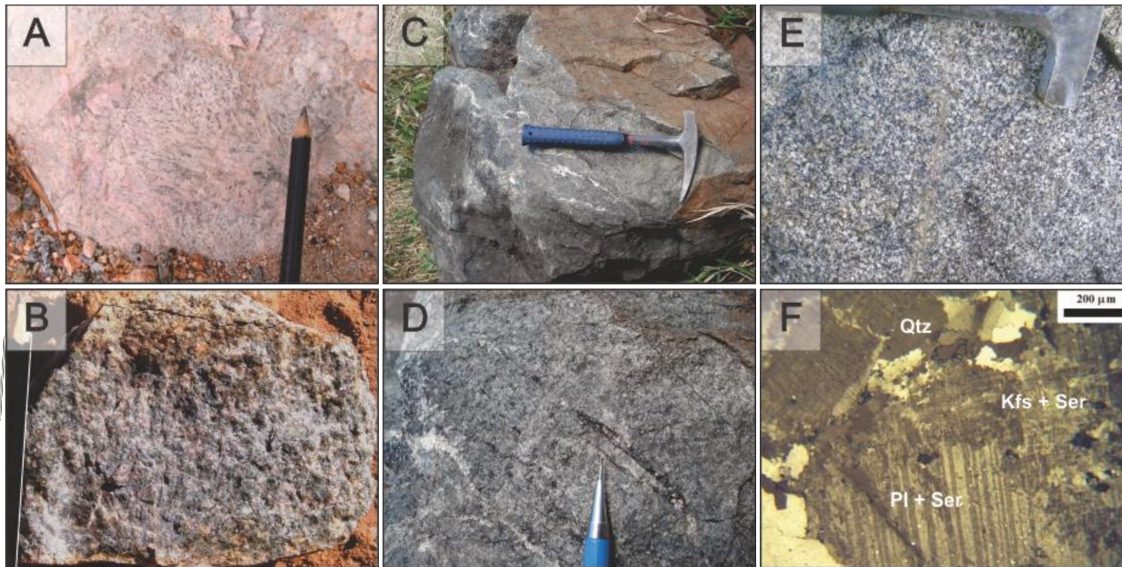


Figure 3 – Features from Alvo Bacaba host rocks. (A) Micrographic texture in the Serra Dourada Granite. (B) Serra Dourada Granite as it occurs in the less hydrothermally altered areas showing preserved phaneritic texture. (C) Bacaba Tonalite cut by veins of quartz and scapolite. (D) Bacaba Tonalite showing veinlets of tourmaline and scapolite. (E) Alkali feldspar vein in the Serra Dourada granite. (F) Serra Dourada Granite in thin section, showing plagioclase partly replaced by potassium feldspar and sericite (TL, CP). Abbreviations: TL – transmitted light, CP – crossed polarizers, Kfs – alkali feldspar, Pl – plagioclase, Qtz – quartz, Ser – sericite.

The Alvo Castanha is mainly hosted by hydrothermally altered subvolcanic acid rocks of rhyolitic to rhyodacitic composition, here named as the Castanha feldspar-quartz porphyry (**Figure 4B**). This rock has a black or dark gray colour and when least-altered is composed of quartz (~45%), plagioclase (~5%), potassium feldspar (~35%), and fine-grained biotite (~10%), even though this proportion varies with the intensity of hydrothermal alteration. These hydrothermally altered rocks can be distinguished by the presence of quartz megacrystals (**Figure 4F**) that show euhedral to sub-euhedral bipiramidal habit with 0.5 to 3 mm in length, which often exhibit features similar to corrosion gulfs. Quartz megacrystals commonly present blue colour due to tiny ilmenite inclusions identified using SEM. Inclusion-rich quartz rims with optical continuity with the megacrystal core (Pestilho and Monteiro 2008) commonly are partially replaced by hydrothermal biotite or potassium feldspar. Plagioclase also occurs as megacrystals

within the rock matrix, especially in the most preserved and distal portions in relation to the copper ore bodies. These plagioclase megacrystals show sub-euhedral habit with albite or chessboard twinning (**Figure 4D**) and 1 to 3.5 mm in length.

The matrix of the Castanha feldspar-quartz porphyry shows fine-grained phaneritic texture with crystals size from 0.1 to 1 mm in length composed of quartz, alkali feldspar and subordinated biotite. Higher biotite content is observed in mylonitized samples, evidencing S–C structures accompanied with crystal stretching and comminuting of quartz and other mineral phases, including scapolite and biotite (Pestilho and Monteiro 2008).

Intrusive basic rocks (**Figure 4A**) occur in both deposits (Augusto *et al.* 2008, Pestilho and Monteiro 2008). These are represented by isotropic gabbro with dark green colour and medium- to fine-grained phaneritic textures. Gabbros of both deposits can be precisely characterized in relatively preserved sections due to the identification of sub-ophitic to ophitic textures (**Figures 4C and 4E**). However, under the microscope its composition consists essentially of hydrothermally altered minerals, such as interstitial amphibole and epidote around plagioclase plates replaced by albite and scapolite. Magnetite and remains of ilmenite are the typical accessory minerals. Augusto *et al.* (2008) described scheelite inclusions into magnetite crystals in the Alvo Bacaba gabbro.

The contact between gabbro and hydrothermally altered granitoids in the Alvo Bacaba, in some cases, is characterized by intense hydrothermal alteration in both rocks concomitant to the ductile shear zones development (Augusto *et al.* 2008). Nevertheless, at the deposit vicinity metagabbro enclaves inside the Bacaba Tonalite was identified. In the Alvo Castanha the contact between the gabbro and the Castanha feldspar-quartz porphyry is not clear while observed in drill core samples.

In minor proportion, brown to reddish acid intrusive rock dykes also occur in both deposits crosscutting all the host rocks, including the Castanha quartz-feldspar porphyry. These rocks in the Alvo Bacaba deposit are designated as quartz-feldspar porphyry (Augusto *et al.* 2008), and have restrict occurrence and variable degree of deformation and hydrothermal alteration. It also presents porphyritic texture with bipiramidal quartz megacrystals and euhedral feldspar crystals. This quartz-feldspar porphyry occurs in the Alvo Castanha as small dykes intensely hydrothermally altered, not foliated, with restricted occurrence and composed of fine-grained biotite and quartz.

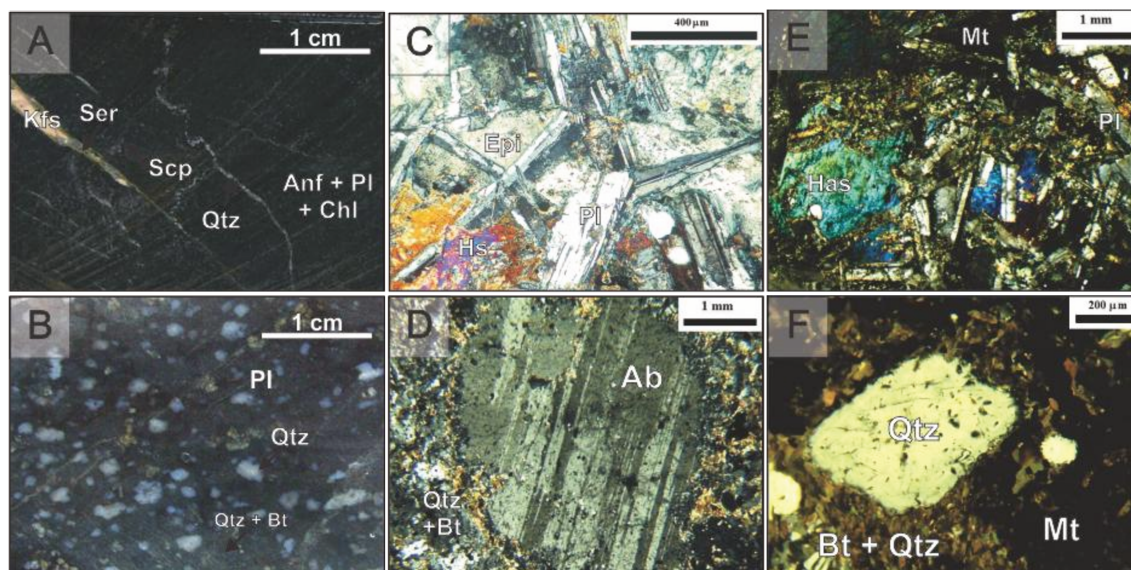


Figure 4 – Features from the Alvo Castanha host rocks. (A) Aspect of the gabbro as it appears in altered drill core samples from the Alvo Castanha deposit. (B) Hydrothermally altered Castanha quartz-feldspar porphyry as it occurs in the nearest areas from the magnetitite orebodies. (C) Relic of igneous texture in gabbro from Alvo Castanha (TL, CP). (D) Albite megacrystal with chessboard texture in the Castanha feldspar-quartz porphyry (TL, CP). (E) Relic of igneous texture in gabbro from Alvo Bacaba (TL, CP). (F) Euhedral quartz megacrystal involved by hydrothermal biotite in the Castanha feldspar-quartz porphyry (TL, CP). Abbreviations: TL – transmitted light, CP – crossed polarizers, Kfs – alkali feldspar, Pl – plagioclase, Qtz – quartz, Ser – sericite.

PARAGENETIC RELATIONSHIPS

Successive hydrothermal alteration stages have been characterized in the Alvo Bacaba and Alvo Castanha deposits and the paragenetic evolution of each deposit is summarized in **Figure 5**. Except the sodic-calcic alteration and expressive magnetite bodies, which are well developed only in the Alvo Castanha deposit, a similar paragenetic succession could be recognized in the two deposits.

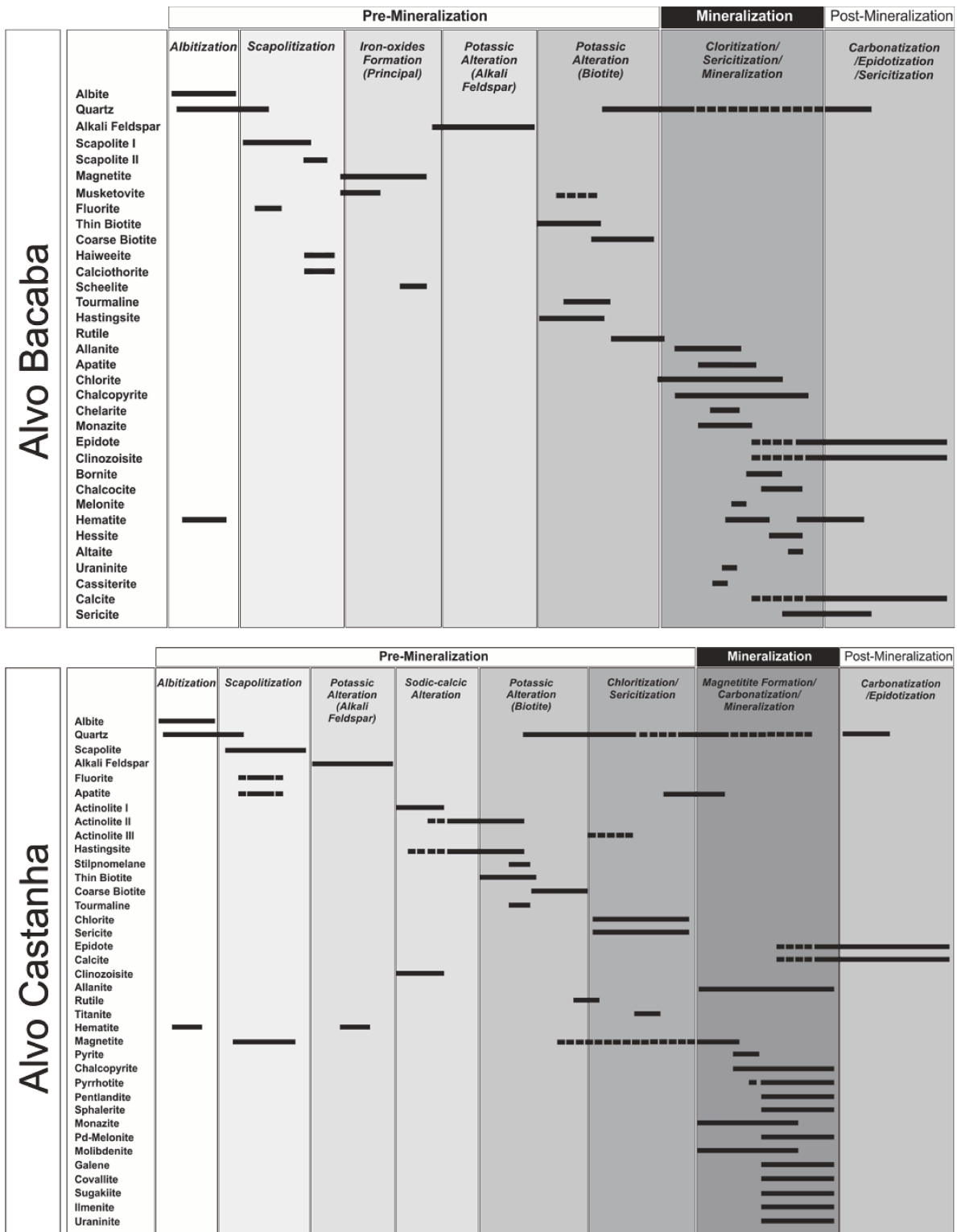


Figure 5 – Alvo Bacaba and Alvo Castanha paragenetic evolution chart (modified from Augusto *et al.* 2008, and Pestilho and Monteiro 2008).

Albite Alteration

Albite alteration represents the earliest hydrothermal alteration stage for both Alvo Bacaba (**Figure 6A**) and Alvo Castanha (**Figure 6B**) deposits, even though later albite veins and veinlets were also reported. In all major host rocks, hydrothermal albite generally presents white to pinkish colour, due to hematite microinclusions.

Under microscopy, hydrothermal albite crystals can be distinguished from igneous plagioclase because they have cleaner aspect and/or show distinct twinning and textures from that of igneous origin. Hydrothermal albite crystals occur as sub-euhedral crystals, generally with albite (**Figure 7A**) or chessboard twinning (**Figure 7B**). In most cases, albite twinning does not show a regular pattern of lamellas, such as in fan texture, especially observed in late veinlets.

Both deposits show albitization strongly obliterated by late alteration stages. Initial albite alteration seems to have been pervasive and it was subsequently replaced by scapolite, biotite, epidote, calcite and chlorite in both deposits. Additionally, substitution by apatite and fluorite was reported in the Alvo Castanha samples.

In the Alvo Bacaba deposit, late hydrothermal albite is associated with ore minerals, such as chalcopyrite, and replaces potassium feldspar (Augusto *et al.* 2008). Late albite in the Alvo Castanha deposit occurs in vein and veinlets, sometimes without twinning, and is associated with chlorite, titanite and carbonate minerals. These veinlets were seldom observed associated with pyrite and chalcopyrite unlike the Alvo Bacaba samples. In this case, albite replaced potassium feldspar and scapolite, and it was substituted by sericite (Pestilho and Monteiro 2008).

Scapolite Alteration

Scapolite is associated mainly with fissural-controlled alteration and associated veinlets, veins and stockworks. These zones of scapolite alteration can be very extensive and they often result in erroneous interpretation of pervasive alteration zones, although disseminated scapolite are also common. Scapolite occurs as fibrous crystals oriented along the mylonitic foliation, showing kinematic indicators and, sometimes, undulatory extinction as observed in coarse-grained scapolite crystals from the Alvo Bacaba.

Scapolite in the Alvo Bacaba is of widespread occurrence and was developed in, at least, two vein generations. Reddish scapolite veins (up to 10 m in width) were crosscut by white scapolite veins with up to 20 cm in width. Under the microscope, the first scapolite generation (SCPI) is represented by coarse-grained fibrous or prismatic crystals with low birefringence, typical of marialite, associated with quartz, magnetite, fluorite and epidote. Veins with SCPI were crosscut by irregular zones of a late scapolite generation (SCPII), which is fine-grained, marialitic, and strongly oriented along foliation (**Figure 7C**). Locally, SCPII composes the matrix around SCPI fragments. Scapolite from veins (SCPI and SCPII) was partially replaced by alkali feldspar, biotite and sericite. Uranium and thorium minerals, such as haiweeite $[\text{Ca}[(\text{UO}_2)_2\text{Si}_5\text{O}_{12}(\text{OH})_2] \cdot 3(\text{H}_2\text{O})]$ and calcliothorite $[(\text{Th},\text{Ca}_2)\text{SiO}_4 \cdot 3.5\text{H}_2\text{O}]$, also fill fractures between fibrous scapolite crystals.

In the Alvo Castanha, scapolite occurs in veins and in biotite-rich altered zones (as seen in **Figure 6B**). In veins, scapolite and fluorite commonly occur in textural equilibrium and are also associated with chalcopyrite and pyrite. Within biotite-rich altered zones, scapolite crystals occur along the foliation as deformed crystals with pressure shadows. Commonly the crystals are zoned showing calcic cores and marialitic rims. Late alteration stages with alkali feldspar, sericite, biotite, actinolite (**Figure 7D**), calcite, and chlorite crosscut scapolite-rich zones.

Sodic-calcic Alteration

Sodic-calcic alteration is associated with actinolite and hastingsite formation. It is a characteristic and selective alteration of gabbros with subophitic to ophitic textures observed in the Alvo Bacaba (Augusto *et al.* 2008) and Alvo Castanha (Pestilho and Monteiro 2008) deposits. In these rocks, hastingsite replaces relicts of igneous augite and occurs in the interstitial spaces between albitized plagioclase laths, which were also partially replaced by clinozoisite. Sodic-calcic alteration is overprinted by potassic alteration and actinolite is replaced by biotite and crosscut by K-feldspar veinlets. Sodic-calcic alteration was also recognized in distal areas in relation to the main copper orebodies in the Alvo Castanha deposit and show close spatial relationship with magnetite-rich zones (**Figure 6D**). In those zones, actinolite occurs in at least three distinct associations and compose intensely altered zones, in which amphibole represents the main mineral phase, named as actinolite zone. These associations include:

ACTI – Coarse-grained actinolite crystals (1 to 3 mm in length) associated with clinozoisite that replace scapolite (**Figure 7D**), albite and bipiramidal quartz megacrystals of the Castanha Porphyry.

ACTII – Fine-grained actinolite crystals (up to 1 mm in length) that partially replace ACTI (**Figure 7F**), scapolite and apatite and, in turn, are associated with biotite, which shows straight boundaries with actinolite crystals. Also actinolite and biotite occur oriented along the same foliation. ACTII occurs associated with hastingsite in two associations: actinolite + biotite + hastingsite or actinolite + hastingsite.

ACTIII – Coarse-grained actinolite crystals with sizes from 1 to 3 mm in length also occur in veinlets and veins with comb texture that crosscut ACTII association.

These distinct associations from the Alvo Castanha deposit were formed in an early alteration stage (ACTI), synchronous to potassic alteration with biotite (ACTII), and in a later alteration stage (ACTIII). Furthermore, some magnetite crystals with scattered occurrence seem to show straight contacts with actinolite crystal from ACTIII, although actinolite generally occurs partially replaced by magnetite, chalcopyrite and associated minerals.

Potassic Alteration (Alkali Feldspar)

Hydrothermal K-feldspar is associated with either pervasive or fissural alteration styles in both Alvo Bacaba (**Figure 6C**) Alvo Castanha (**Figure 6F**) deposits. Potassium feldspar occurs as sub-euhedral crystals without any twinning and/or with microcline twinning, being also partially or completely sericitized. Alkali feldspar crystals exhibit association with very fine hematite crystals, smaller than 10 μm , that show ruby-red internal reflexes under reflected light and occur as scattered clusters between the feldspar crystals and in fractures within the alkali feldspar crystal boundaries.

Veins and veinlets with alkali feldspar crosscut zones with albite, scapolite and some magnetite veins, being generally prior to the main ore formation stage. Within pervasive potassic alteration zones, scapolite crystals are partially replaced by alkali feldspar. Also in these zones alkali feldspar was partially replaced by biotite from a clear later pervasive alteration. Commonly, feldspar occurs intensely sericitized.

Structurally-controlled potassic alteration zones in the Alvo Bacaba deposit associated to mylonitic foliation is represented by K-feldspar associated with rutile or with calcite \pm musketovite (hematite replaced by magnetite) \pm hematite \pm chalcopryrite. Also at Alvo Bacaba, alkali feldspar veins and veinlets commonly show an external halo with chlorite and calcite.

In both Alvo Bacaba and Alvo Castanha deposits, late veins and veinlets with K-feldspar also crosscut biotite-rich zones, and in some cases these feldspar crystals were also replaced by biotite (**Figure 6E**).

Potassic Alteration with Biotite

Biotite-rich potassic alteration occurs in very extensive and pervasive zones (**Figure 6 and Figure 8**). Disseminated biotite occurs as brown lamellar crystals, mainly sub-euhedral, with sizes from 1 μm , associated with quartz, magnetite, alkali feldspar, scapolite (**Figures 9A and 9B**), zircon and rarely chalcopyrite and pyrite in pervasive alteration zones.

In the proximal areas from the pyrrhotite-rich copper ore from the Alvo Castanha, there is a common association of biotite and brown stilpnomelane. Also in the Alvo Castanha, biotite is associated with actinolite and hastingsite (ACTII). The relationship between actinolite and biotite suggests that some crystals formed in textural equilibrium, so that some biotite crystals show straight boundaries with actinolite crystals (Pestilho and Monteiro 2008).

Generally, fine-grained biotite crosscut and replaces scapolite-rich rocks as well as potassic altered zones with K-feldspar. However, late alkali feldspar veins also crosscuts biotite-rich zones. Late biotite veins with coarser crystals (up to 1 mm in length) associated with quartz (**Figure 8B**) are also typical of both deposits, and generally they crosscut pervasive zones with fine-grained disseminated biotite.

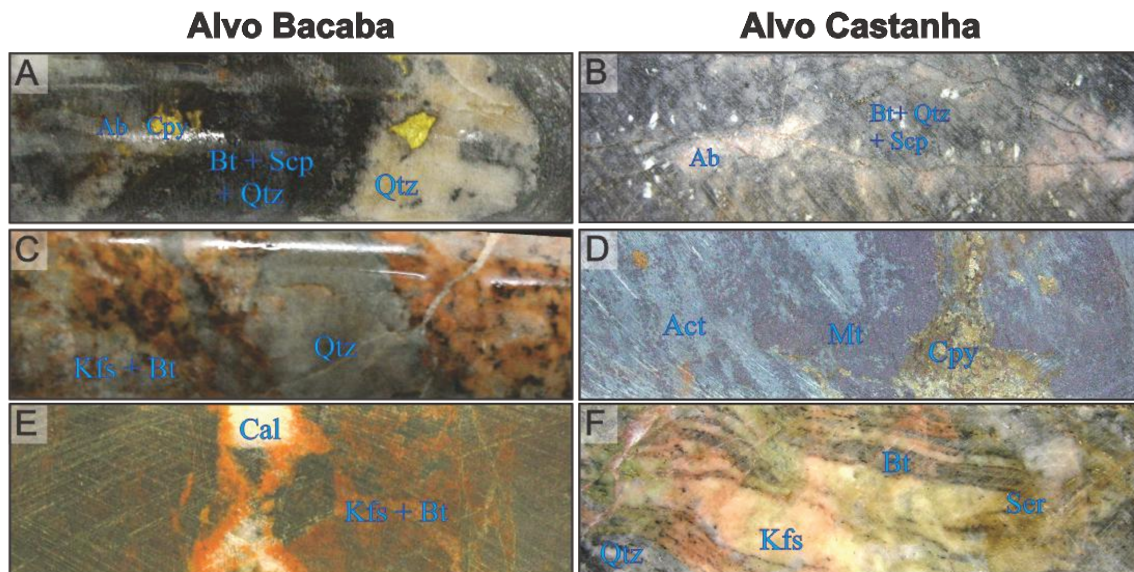


Figure 6 – Drill core samples from Alvo Bacaba and Alvo Castanha showing hydrothermal alteration features. All samples have 2.5 cm height. (A) Albite vein partially replaced by pervasive potassic alteration zone with biotite associated with disseminated scapolite crystals. Post potassic alteration quartz vein associated with

chalcopyrite are also displayed. (B) Albite alteration replaced by scapolite alteration and pervasive potassic alteration with biotite, respectively. (C) Potassic feldspar associated with biotite and quartz veins. (D) Magnetite and actinolite overprinted by copper mineralization (E) Association of potassic feldspar, biotite and calcite. (F) Potassic feldspar associated to biotite, sericite and quartz. Abv: Ab – albite, Bt – biotite, Cal – calcite, Kfs – alkali feldspar, Cpy – chalcopyrite, Qtz – quartz, Ser – sericite, Scp – scapolite.

Tourmaline Formation

The association between biotite and subeuhedral dark greenish-blue tourmaline (**Figures 9C and 9D**) is common, especially in distal biotite-rich zones relative to the Castanha orebodies. Nevertheless, the higher tourmaline content (up to 30% molar volume) was reported in the Alvo Bacaba deposit by Augusto *et al.* (2008) in altered zones developed along the mylonitic foliation. In those zones, tourmaline occurs associated with scapolite (SCPI and SCPII) and reveal mutual replacement by biotite.

Chloritic Alteration

In the Alvo Bacaba, chlorite replaces disseminated biotite from pervasive potassic alteration zones and it occurs in veinlets crosscutting alkali feldspar, albite, biotite, scapolite (**Figure 8A**) and amphibole. It is remarkable that some minerals were totally replaced by chlorite polymorphs, while others stood almost completely preserved in the same associations. That is the case of scapolite crystals that generally occurs chloritized associated with non-altered biotite.

Sericitic Alteration

Sub-euhedral to anhedral sericite crystals occur associated with quartz \pm alkali feldspar (**Figure 8C**) and rarely in association with chalcopyrite and biotite. Sericite veinlets also crosscut the biotite \pm quartz \pm scapolite (**Figure 8D**) association. Sericite alteration at Alvo Castanha was less expressive than in the Alvo Bacaba and developed mainly in distal areas from the pyrrhotite-rich copper mineralized zones, whereas in proximal to the magnetite bodies, sericite occurs associated to alkali feldspar \pm magnetite.

Carbonate and Epidote Alteration

Rare late calcite veinlets and veins (calcite \pm alkali feldspar \pm musketovite \pm hematite (**Figure 9E**) or only calcite \pm hematite) are recognized in the Alvo Bacaba deposit.

In the Alvo Castanha, pervasive and fissure-controlled carbonate alteration was more widespread than in the Alvo Bacaba. In veins and veinlets (**Figure 9F**), calcite is associated with sulfides \pm epidote \pm chlorite and occur cutting through all the previous minerals. Pervasive carbonate alteration is closely related to pyrrhotite-rich copper orebodies. Calcite, REE-bearing carbonates, and epidote also occur in breccia matrix enclosing magnetite, chalcopyrite and pyrite in distal zones from the pyrrhotite-rich copper orebodies.

Iron Oxide Formation

Iron oxides occur in distinct associations in both Alvo Bacaba and Alvo Castanha deposits, evidencing that these hydrothermal oxides were not formed in a single event. These iron oxide associations represent the main distinguishing feature between these deposits, besides the copper ore characteristics.

In the Alvo Bacaba, early magnetite occurs as euhedral to sub-euhedral crystals infilling fractures in scapolite (SCPI) crystals from veins and along the mylonitic foliation as elongated magnetite crystals. In intensely mylonitized scapolite zones, magnetite relics occur as smaller xenomorphic crystals associated to Fe-Ti-(Mn) oxides and goethite. In this deposit, a large amount of disseminated magnetite associated with alkali feldspar replaced the host rocks, forming magnetitites, which are in turn crosscut by K-feldspar veinlets.

In the Bacaba ore bodies, lamellar musketovite has been identified, suggesting that previous hematite was replaced by magnetite resulting in a pseudomorph. Some hematite crystals were totally replaced by magnetite, as well as musketovite. However, late hematite is also observed along fracture or rims of the musketovite crystals. Euhedral hematite lamellas in straight contact with chalcopyrite are also associated with the Alvo Bacaba ore.

In the Alvo Castanha, minor magnetite occurs associated with scapolite veins. Magnetite also occurs as sub-euhedral to euhedral crystals associated with chalcopyrite and pyrite in distal veinlets from the main mineralized zones. However, larger amounts of magnetite occur as disseminated crystals associated with chalcopyrite and pyrrhotite within carbonate altered and mineralized zones.

In distal portions of the Alvo Castanha deposit in relation to the main pyrrhotite-rich orebodies, magnetite-rich zones are associated with sodic-calcic alteration, mainly with actinolite bodies. These zones are represented by magnetite in different associations: (I) disseminated fine-grained sub-euhedral crystals associated with the least-altered Castanha Porphyry or associated with actinolites; or (II) magnetite (up to 85%) associated with apatite + monazite ± actinolite ± chlorite ± calcite ± biotite ± pyrite ± chalcopyrite forming massive magnetite bodies, as seen in **Figures 7D** and **8B**.

In the association (I), disseminated magnetite partially replaces actinolite, and also magnetite crystals occur with straight boundaries with actinolite crystals, whereas in the association (II), calcite and chlorite fill fractures in magnetite crystals and replaces apatite. Apatite is partially replaced by stilpnomelane, which in turn occur in straight contacts with monazite. Magnetite in the association (II) is later than all other hydrothermal mineral phases, except chlorite and stilpnomelane.

Silicification

Silicification occurs in both deposits as a pervasive and mainly fissural style of alteration. Different generations of quartz veins and veinlets are composed of crystals with sizes from < 1 mm to about 1 cm or more, and associated with: (I) early albite, scapolite and biotite; (II) late sericite; and (III) pyrite and chalcopyrite.

Pervasive silicification zones overprint early albitization in the Alvo Bacaba host rocks. In the Alvo Castanha, pervasive silicification zones are associated with biotite from potassic alteration, or combined with chalcopyrite that occur disseminated in the magnetite and actinolite-rich bodies.

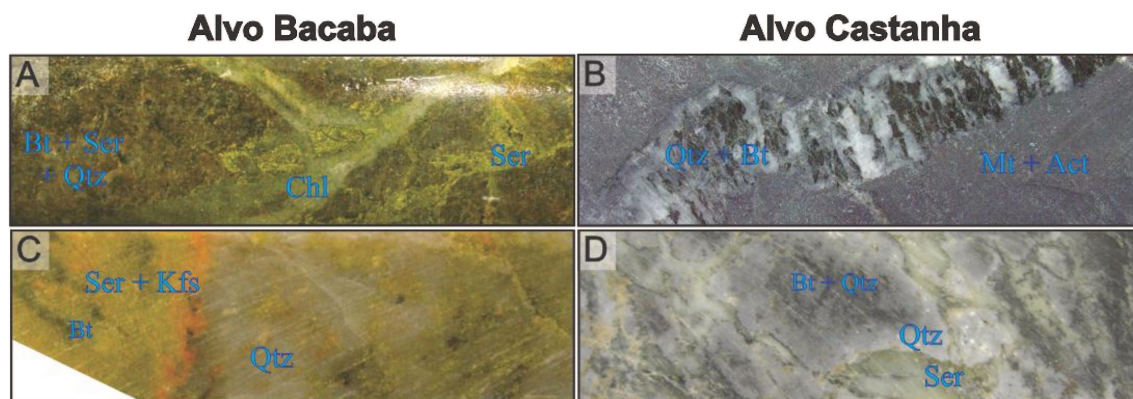


Figure 7 – Drill core samples from Alvo Bacaba and Alvo Castanha showing hydrothermal alteration features. All samples have 2.5 cm height. (A) Chlorite veins crosscut potassic alteration. Chlorite shows association with sericite. (B) Magnetite crosscut by quartz+biotite vein showing comb texture. (C) Partially overprinted potassic feldspar and biotite by sericite and quartz. (D) Sericite replacing biotite-rich potassic altered rock. Abbreviations: TL – transmitted light, CP – crossed polarizers, PP – parallel polarizers, Ab – albite, Bt – biotite, Cal – calcite, Chl – chlorite, Hs – hastingsite, Kfs – alkali feldspar, Qtz – quartz, Ser – sericite, Scp – scapolite, Tur – tourmaline.

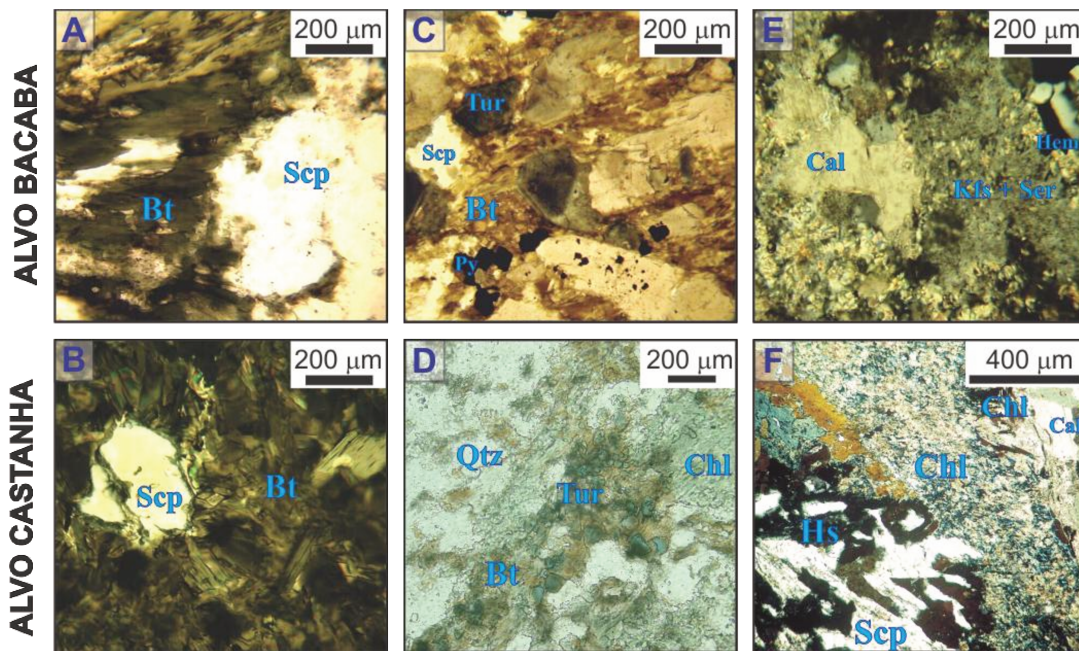


Figure 8 – Hydrothermal alteration assemblages from Alvo Castanha: (A) and (B) show scapolite partially replaced by biotite from both deposits. (C) Tourmaline, biotite, scapolite and pyrite association (LT, CP). (D) Mineral association composed of biotite, tourmaline, quartz and chlorite (TL, PP). (E) Calcite, alkali feldspar, sericite and hematite within alkali feldspar veins (TL, CP). (F) Calcite vein with chlorite pseudomorphs (with biotite habit), chlorite, hastingsite and scapolite inclusions (TL, CP). Abbreviations: TL – transmitted light, CP – crossed polarizers, PP – parallel polarizers, Ab – albite, Bt – biotite, Cal – calcite, Chl – chlorite, Hs – hastingsite, Kfs – alkali feldspar, Qtz – quartz, Ser – sericite, Scp – scapolite, Tur – tourmaline.

Copper Ore Zone

In the Alvo Bacaba, sulfides occur as veinlets, veins and mineralized breccias (**Figures 10A and 10B**) in structurally-controlled replacement zones up to 30-cm thick along the mylonitic foliation. Chalcopyrite (**Figure 10C**) represents the principal ore mineral and occurs associated with bornite (**Figure 10D**) and pyrite.

Mineralized zones show spatial relationship with zones of potassic alteration with alkali feldspar, which is crosscut by mineralized veins with chalcopyrite accompanied by chlorite, calcite, epidote, clinozoisite, allanite, apatite, monazite, rutile, magnetite/musketovite (**Figure 10E**), and hematite (**Figure 10F**). Commonly, a thin albite-rich halo (up to 1 mm) separated the K-feldspar crystals from the crosscutting sulfides.

Melonite (NiTe_2) and altaite (PbTe) are important accessory phases of the Bacaba mineralized zones, which fill fractures or represent mineral inclusions into chalcopyrite or gangue minerals. Other accessory minerals are represented by galena, uraninite, hessite, cheralite [$\text{CaTh}(\text{PO}_4)_2$], olsacherite ($\text{Pb}_2\text{SO}_4\text{SeO}_4$), and tsumoite (BiTe), which occur as thin inclusions in chalcopyrite. Hessite occurs associated with melonite in chalcopyrite edges, whereas olsacherite were identified as needles in fractures walls within chalcopyrite crystals (Augusto *et al.* 2008).

In the Alvo Castanha, the copper orebodies occur with two distinct associations: (I) chalcopyrite (up to 75%) + pyrite (up to 25%) \pm molybdenite + quartz + monazite + magnetite, which occur associated with the magnetite and actinolite bodies; (II) chalcopyrite + pyrrhotite + pyrite + sphalerite + marcasite in the richest and more extensive ore bodies.

The ore association (I) occurs mainly in veins and veinlets that crosscut the hydrothermally altered Castanha Porphyry, and in magnetite or actinolite or within structurally-controlled breccias with magnetite fragments and magnetite crystals. Chalcopyrite-epidote-magnetite-allanite veinlets also crosscut sodic-calcic alteration. In contrast with association (II), in the association (I) there is no occurrence of large amount of calcite with the ore bodies, and calcite occurs as a minor phase associated with epidote and accessory minerals.

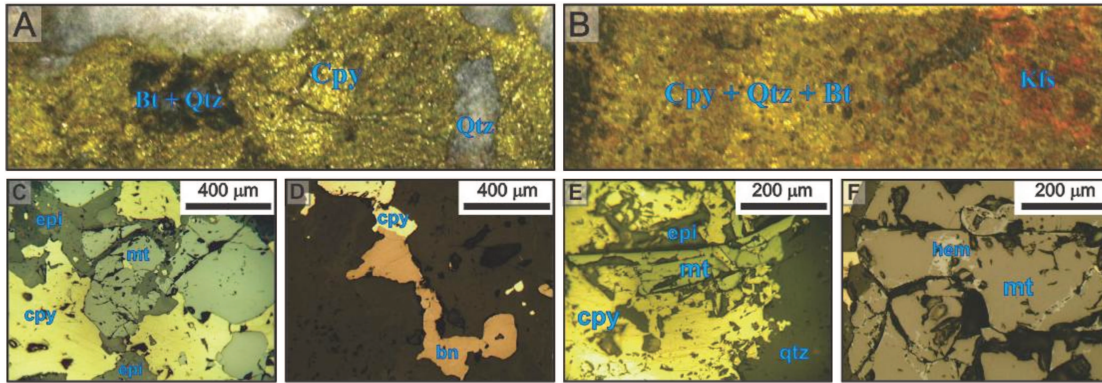
In the main mineralized zone of the Alvo Castanha deposit, ore occurs in veins, veinlets, stockwork and breccias (**Figure 10G and 10H**). Transition zones between vein stockwork and breccia zones have matrix composed of ore minerals. Mineralized breccias are also structurally-controlled and present deformed clasts of altered host rocks. The estimated mineral abundances

in association (II) are chalcopyrite (~ 35%), pyrite (~15%; **Figure 10I**) and pyrrhotite (~50%; **Figure 10J**).

Also in the mineralized zone with the association (II), veins and veinlets are composed of sub-euhedral to euhedral pyrite crystals, generally associated with chalcopyrite, quartz, calcite, albite, scapolite, Cl-apatite, fluorite, and magnetite. In the breccias matrix, pyrrhotite occurs associated with chalcopyrite, pyrite, sphalerite (**Figure 10K**), and minor marcasite. However, direct contact between pyrite and pyrrhotite was not observed. The breccia lithic clasts within the ore breccia comprises host rocks replaced by biotite, chlorite, allanite, stilpnomelane, calcite and REE-bearing carbonate minerals. Allanite occurs as zoned euhedral crystals included in pyrrhotite and calcite, and it is rarely found chloritized.

In the mineralized zone from association (II) it was also identified a variety of accessory minerals that includes: uraninite, galena, monazite [(Ce,La,Nd)_{0.94}P_{1.04}O₄], pentlandite, Copentlandite [(Ni,Co,Fe)_{9.20}S_{8.39}], Pd-melonite [(Fe,Ni,Pd)_{0.31}Te_{0.61}], sugakiite [Cu_{0.66}(Fe,Ni)_{8.4}S_{8.42}], Ni-pyrite [(Fe,Ni)_{0.79}S_{1.72}], molybdenite (Mo_{0.34}S_{2.06}). Copentlandite and pentlandite are commonly associated with pyrrhotite and occur as inclusions or at the pyrrhotite crystal edges, where they have granular or flame textures (**Figure 10L**). Pd-melonite was observed as thin crystals included in pyrrhotite. Uraninite occurs in both host rock clasts and as small (~1 µm) anhedral inclusion in sulfides. Similarly galena occurs as small anhedral crystals (~1 µm) disseminated in the lithic fragments within the breccias in the mineralized zones, and rarely occurs associated with sphalerite. Monazite was observed in the Cl-apatite edges, whereas euhedral molybdenite crystals occur as inclusion in Cl-apatite and allanite (Pestilho and Monteiro 2008).

Alvo Bacaba



Alvo Castanha

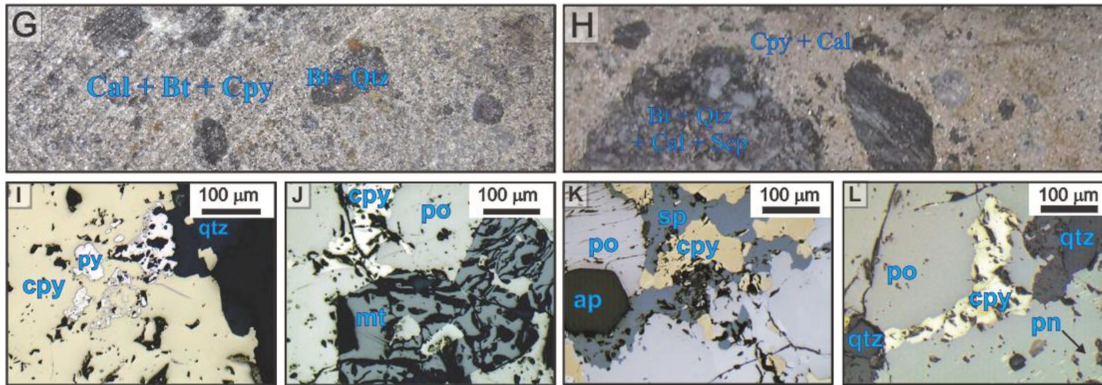


Figure 9 – Ore mineral association in Alvo Bacaba and Alvo Castanha. All drill core samples have 2.5 cm height. All thin section images were taken in reflected light with parallel polarizers. (A) and (B) show Alvo Bacaba mineralized breccias with matrix mainly composed of chalcopyrite associated with quartz, biotite and specially potassic feldspar clasts. (C) Chalcopyrite and magnetite partially substituted by hematite. (D) Bornite and chalcopyrite association. (E) Magnetite with tabular habit (probably musketovite) associated with chalcopyrite. (F) Magnetite partially replaced by hematite. (G) and (H) show mineralized breccias with matrix mainly composed by pyrrhotite, chalcopyrite and calcite with biotite+quartz+/-scapolite clasts. (I) Pyrite and chalcopyrite association in quartz veins distal in relation to the mineralized breccia bodies. (J) Chalcopyrite, pyrrhotite and magnetite association, showing pyrrhotite inside of magnetite fractures. (K) Mineralized breccia showing association among sphalerite, chalcopyrite and pyrrhotite. (L) Pentlandite flame texture indicated by a dark arrow, in pyrrhotite, associated to chalcopyrite in ore breccias. Abbreviations: ap – apatite, bn – bornite, bt – biotite, cal – calcite, cpy – chalcopyrite, hem – hematite, mt – magnetite, po – pyrrhotite, pn – pentlandite, py – pyrite, qtz – quartz, scp – scapolite.

5. CARBON, OXYGEN AND HYDROGEN STABLE ISOTOPES

The $\delta^{18}\text{O}_{\text{V-SMOW}}$ values were obtained for actinolite (Alvo Castanha or AC – 6.9‰ to 7.3‰, n= 2), biotite (Alvo Bacaba or AB – 2.8‰ to 3.0‰, n=2; AC – 4.88‰ to 5.5‰, n=4), chloritized biotite (AB – 2.5‰, n=1), calcite (AB – 8.31‰ to 17.3‰, n=5; AC – 6.04‰ to 10.88‰, n=11), alkali feldspar (AB – 5.8‰ to 8.3‰, n=4; AC – 7.1‰ to 7.4‰; n=2), hematite (AB – -10.8‰ to 7.0‰, n=2), magnetite (AC – -1.5‰ to 1.4‰, n=3), musketovite (AB – -6.9‰ to -2.7‰, n=2), quartz (AB – 8.9‰ to 9.4‰, n=5; AC – 10.6‰ to 11.5‰, n=5), and sericite (AB – 4.2‰ to 7.6‰, n=3; AC – 3.5‰ to 8.0‰, n=2). The $\delta^{13}\text{C}_{\text{PDB}}$ values obtained in calcite for the Alvo Bacaba deposit varies from -3.63‰ to -5.62‰, whereas for the Alvo Castanha deposits the $\delta^{13}\text{C}_{\text{PDB}}$ values range from -3.34‰ to -7.1‰. The **table 1** shows all δD and $\delta^{18}\text{O}$ data for silicates and oxides, while **table 2** shows $\delta^{13}\text{C}$ and $\delta^{18}\text{O}$ data for calcite and **Table 3** present $\delta^{34}\text{S}$ data for sulfides.

Table 1 – Oxygen and hydrogen isotopic data for hydrothermal silicates and oxides of the Alvo Bacaba and Alvo Castanha deposits.

SAMPLE	MINERAL	$\delta^{18}\text{O}_{\text{V-SMOW}} (\text{‰})$	$\text{H}_2\text{O}^+ \mu\text{molesmg}^{-1}$	$\delta\text{D}_{\text{V-SMOW}} (\text{‰})$
ALVO BACABA				
BAC 25/341.85	Musketovite	-7.6; -6.9		
BAC 28/100.70	Musketovite	-2.8; -2.7		
BAC 28/100.70	Hematite	-7.0		
BAC 26/240.2	Hematite	-10.8		
BAC 25/345.75	Quartz	9.4		
BAC 03/210.0	Quartz	9.0		
BAC 25/342.3	Quartz	9.4		
BAC 13/78.03	Quartz	8.9		
BAC 25/297.45	K-Feldspar	9.0; 8.3		
BAC 04/104.4	K-Feldspar	8.4		
BAC 03/210.0	K-Feldspar	5.8		
BAC 25/46.6	K-Feldspar	7.7		
BAC 25/341.85	K-Feldspar	7.3; 7.6		
BAC 25/297.45	Sericite	7.6		
BAC 25/211.8	Sericite	7.5	2.6	-52
BAC 03/210.0	Sericite	4.2	2.0	-52
BAC 25/341.25	Chlorite	2.5		
BAC 25/341.25	Biotite	2.8	2.8	-84
BAC 03/41.46	Biotite	3.0	2.3	-104

SAMPLE	MINERAL	$\delta^{18}\text{O}_{\text{V-SMOW}} (\text{‰})$	$\text{H}_2\text{O}^+ \mu\text{molesmg-1}$	$\delta\text{D}_{\text{V-SMOW}} (\text{‰})$
ALVO CASTANHA				
CTND 01/59.78	Magnetite	1.4		
CTND 02/358.16	Magnetite	-0.2		
CASD 03/216.57	Magnetite	-1.5		
CASD 01/69.9	Quartz	11.5		
BAC 03/41.46	Quartz	9.3		
CTND 09/174.78	Quartz	10.7		
CTND 02/245.7	Quartz	10.9		
CTND 02/320.2	Quartz	11.1		
CTND 02/399.43	Quartz	10.6		
CASD 02/352.0	Quartz	10.9		
CTND 02/399.33	Quartz	10.7		
CATD 09/322.0	K-Feldspar	7.4		
CASD 03/216.57	K-Feldspar	7.1		
CASD 01/69.9	Sericite	8.0	1.3	-71
CATD 09/322.0	Sericite	3.5		
CTND 02/368.70	Actinolite	6.9	1.5	-99
CTND 02/358.16	Actinolite	7.3	1.2	-104
CTND 02/245.7	Biotite	5.5	1.8	-86
CASD 02/352.0	Biotite	4.9	2.6	-100
CTND 02/320.2	Biotite	4.9		

Table 2 – Oxygen and carbon isotopic data acquired from calcite samples of the Alvo Bacaba and Alvo Castanha deposits.

SAMPLE	$\delta^{13}\text{C}_{\text{PDB}} (\text{‰})$	$\delta^{18}\text{O}_{\text{PDB}} (\text{‰})$	$\delta^{18}\text{OSMOW} \text{‰}$
ALVO BACABA			
BAC25/46.6	-5.29	-13.32	17.13
BAC25/211.8	-5.62	-16.48	13.88
BAC25/341.85	-3.63	-21.88	8.31
BACD26/240.20	-4.95	-13.12	17.33
ALVO CASTANHA			
CASD02/267.40	-5.24	-20.18	10.06
CASD02/102.2	-7.01	-21.82	8.37
CATD09/218.00	-4.36	-21.47	8.73
CATD09/242.15	-3.69	-23.21	6.94
CTND01/59.78	-3.34	-19.39	10.88
CTND09/174.78	-3.81	-22.11	8.07

Table 3 – Sulfur isotopic data for the Alvo Bacaba and Alvo Castanha deposits, and other copper deposits of the Transition Domain, Carajás Mineral Province.

SAMPLE	MINERAL	$\delta^{34}\text{S}_{\text{CDT}}$ (‰)
ALVO BACABA		
BACD03/47.10	Chalcopyrite	1.4
BACD03/94.25	Chalcopyrite	1.3
BACD25/342.5	Chalcopyrite	5.1
BACD25/342.5	Chalcopyrite	5.4
BACD25/226.3	Chalcopyrite	1.6
ALVO CASTANHA		
CASD01/121.6	Pyrrhotite	1.3
CASD01/190.65	Pyrrhotite	1.5
CASD02/524.80	Pyrrhotite	1.3
CASD02/567	Chalcopyrite	1.1
CASD02/567	Pyrrhotite	1,0
CTND01/79.0	Chalcopyrite	1.3
CTND 02/18.40	Chalcopyrite	0.8
CTND02/320.4	Chalcopyrite	0.1
CTND02/399.43	Chalcopyrite	0.2
ALVO BACURI		
BRID 07/79. 42	Chalcopyrite	1.1
BRID 05/169.3	Chalcopyrite	- 0.8
BRID05/207.85	Chalcopyrite	0.8
PEDRA BRANCA		
NCN 02/193.8	Chalcopyrite	2.6
XCN18/264.3	Chalcopyrite	2.7
ALVO VISCONDE		
Visconde	Chalcopyrite	1.5
GARIMPOS		
GARIMPO 11	Chalcopyrite	1.7
GARIMPO 18	Chalcopyrite	1.3
GARIMPO 41	Chalcopyrite	1.2

ALVO 188		
FGT13/132.63	Chalcopyrite	3.75
FGT345/127.39	Chalcopyrite	3.28
FGT394/259.00	Chalcopyrite	3.59
FGT394/265.70	Chalcopyrite	4.11
FGT441/300.70	Chalcopyrite	4.16
FGT441/342.70	Chalcopyrite	3.98
FGT441/353.50	Chalcopyrite	4.48
FGT443/187.20	Chalcopyrite	3.76
FGT443/196.30	Chalcopyrite	4.33
FGT453/255.00	Chalcopyrite	3.71

The δD_{V-SMOW} values were obtained for hydrated minerals, including actinolite (AC – -104.0‰ to -99.0‰, n=2), biotite (AB – -104.0‰ to -84.0‰, n=2; AC – -100.0‰ to -86.0‰, n=2), and sericite (AB – -52.0‰, n=2; AC – -69.0‰, n=1).

Actinolite and magnetite were sampled from the actinolite + magnetite association (ACTII) from the Alvo Castanha deposit. In this deposit, magnetite was also sampled from magnetite bodies associated with the main iron oxide formation stage.

Biotite and associated quartz were sampled in both deposits and are related with potassic alteration with biotite-rich zones. Sericite, quartz and alkali feldspar were also sampled in both deposits from the association sericite \pm quartz \pm alkali feldspar, which represent the sericite alteration stage.

Additionally, calcite, alkali feldspar, hematite and/or musketovite were sampled from the associations: (1) veins with alkali feldspar \pm hematite/musketovite \pm chalcopyrite; (2) veins with calcite that crosscut alkali feldspar \pm hematite/musketovite \pm chalcopyrite; (3) calcite veins with calcite and hematite/musketovite; (4) veins with calcite associated or not with quartz \pm chalcopyrite; (5) veins with calcite and biotite. The calcite from associations (1), (2), and (3) were sampled in veins from Alvo Bacaba, whereas the associations (4) and (5) were sampled in the Alvo Castanha deposit.

In the Alvo Bacaba the association (1) was previous (or partially coeval) to the main mineralization event, while the associations (2) and (3) were possibly late to the main mineralization event. In the Alvo Castanha, the association (4) is possibly synchronous or later to

ore deposition, whereas the association (5) is associated with magnetites and might be previous or concomitant to the mineralization stage.

5.1. PALEOTHERMOMETRY AND HYDROTHERMAL FLUID ISOTOPIC COMPOSITION

The **Table 4** shows the mineral pairs that appear to have formed in isotopic equilibrium and allowed temperature calculations based on the isotopic fractionation factors defined by Zheng (1991, 1993a, 1993b, 1994) and Sharp & Kirschner (1994).

Table 4 – Estimated temperature from mineral pairs in isotopic equilibrium from the Alvo Bacaba and Alvo Castanha deposits. Abbreviations: Act – actinolite, Bt – biotite, Cc – calcite, Qtz – quartz, Mt – magnetite.

Deposit	Hydrothermal Alteration stage	Sample	Mineral Pair	Temperature (°C)	Error (°C)	Fractionation Factor
Alvo Bacaba	Potassic Alteration (Biotite)	BACD 03/41.46	Qtz-Bt	355	101	Zheng (1993b)
	Sericite alteration	BACD 03/210	Qtz-Ser	311	96	
Alvo Castanha	Potassic Alteration (Biotite)	CASD 02/352	Qtz-Bt	376	97	Zheng (1993b)
		CTND 02/245.7	Qtz-Bt	422	101	
		CTND 02/320.2	Qtz-Bt	362	96	
		CASD 02/353b*	Qtz-Bt	346	95	
	Sodic-calcic alteration / Magnetite Formation	CTND 02/358.16	Act-Mt	350	93	
	Sericite formation	CASD 01/69.90	Qtz-Ser	447	115	
	Potassic Alteration (K-Feldspar) / Magnetite Formation	CASD03/216,57	Mt-Kfs	479	78	
Carbonate alteration	CTND 01/59.78	Cc-Mt	411	71	Zheng (1991,1994)	
Late carbonate alteration	CTND 09/174.78	Qtz-Cc	302	86	Sharp & Kirschner (1994)	

Oxygen isotopic compositions of the hydrothermal fluid in equilibrium with analysed mineral phases were estimated based on calculated temperatures. These values (**Table 5**) were calculated based on oxygen isotopic fractionation factors between mineral–H₂O for the following minerals: magnetite–H₂O (Zheng 1991), hematite–H₂O (Zheng 1991), alkali feldspar–H₂O (Zheng 1993a), quartz–H₂O (Zheng 1993a), actinolite–H₂O (Zheng 1993b), biotite–H₂O (Zheng 1993b), muscovite–H₂O (Zheng 1993b), calcite–H₂O (Zheng 1994).

The hydrogen isotopic composition of the hydrothermal fluid was calculated using the isotopic fractionation factors for biotite–H₂O (Suzuoki and Epstein 1976), muscovite– H₂O (Suzuoki and Epstein 1976), and actinolite–H₂O (Graham *et al.* 1984).

Table 5 – Estimates of fluid isotopic compositions based on calculated temperatures for different alteration stages of the Alvo Bacaba and Castanha deposits. Note: ^a – Estimates do not consider analytical error and deviation from these values do not represent error. ^b – V-SMOW standard. ^c – PDB standard.

	Hydrothermal alteration stage	Mineral	T (°C) ^a	δ ¹⁸ O _{H2O} (‰) ^{a,b}	δD _{H2O} (‰) ^{a,b}	δ ¹³ CH ₂ C ₃ (‰) ^{a,c}
Alvo Bacaba	Hematite Formation	Hm I	90 ± 10	4.1 ± 0.4		
		Hm II	190 ± 40	0.4 ± 0.1	-	-
	Carbonate alteration	Cc I		1.8 ± 0.5	-	-4.8 ± 0.1
		Cc II	225 ± 5	7.1 ± 0.2	-	-3.0 ± 0.3
		Cc III		10.5 ± 0.3	-	-4.3 ± 0.3
Potassic alteration (Biotite)	Bt	420 ± 10	5.1 ± 0.3	-51 ± 11	-	
Potassic alteration (K-feldspar)	Kfs	450 ± 50	6.2 ± 1.0	-	-	
Sericite alteration	Ser I		3.4 ± 1.4	-17 ± 8	-	
	Ser II	370 ± 50	7.1 ± 0.7	-17 ± 8	-	
Alvo Castanha	Carbonate alteration	CIV		5.2 ± 1.0		-2.8 ± 1.8
		CV		6.3 ± 1.1		-1.5 ± 0.6
		CVI	400 ± 50	7.3 ± 1.0	-	-1.9 ± 0.2
		CVII		8.1 ± 0.8		-2.0 ± 0.8
	Carbonate alteration (in equilibrium with magnetite)	-	417 ± 12	9.5 ± 0.5	-	-0.7
	Sodic-Calcic Alteration/ Magnetite Formation	-	345 ± 25	7.7 ± 0.5	-72 ± 2	-
	Potassic Alteration (Biotite)	BI	440 ± 20	7.5 ± 0.4	-59 ± 3	-
BII		525 ± 25	8.1 ± 0.3	-54 ± 2	-	
Potassic Alteration (K-Feldspar)	-	450 ± 50	5.6 ± 0.7	-	-	
Sericite alteration	SIII	500 ± 50	4.2 ± 0.3	-	-	
	SIV	525 ± 25	8.7 ± 0.3	-55 ± 2	-	

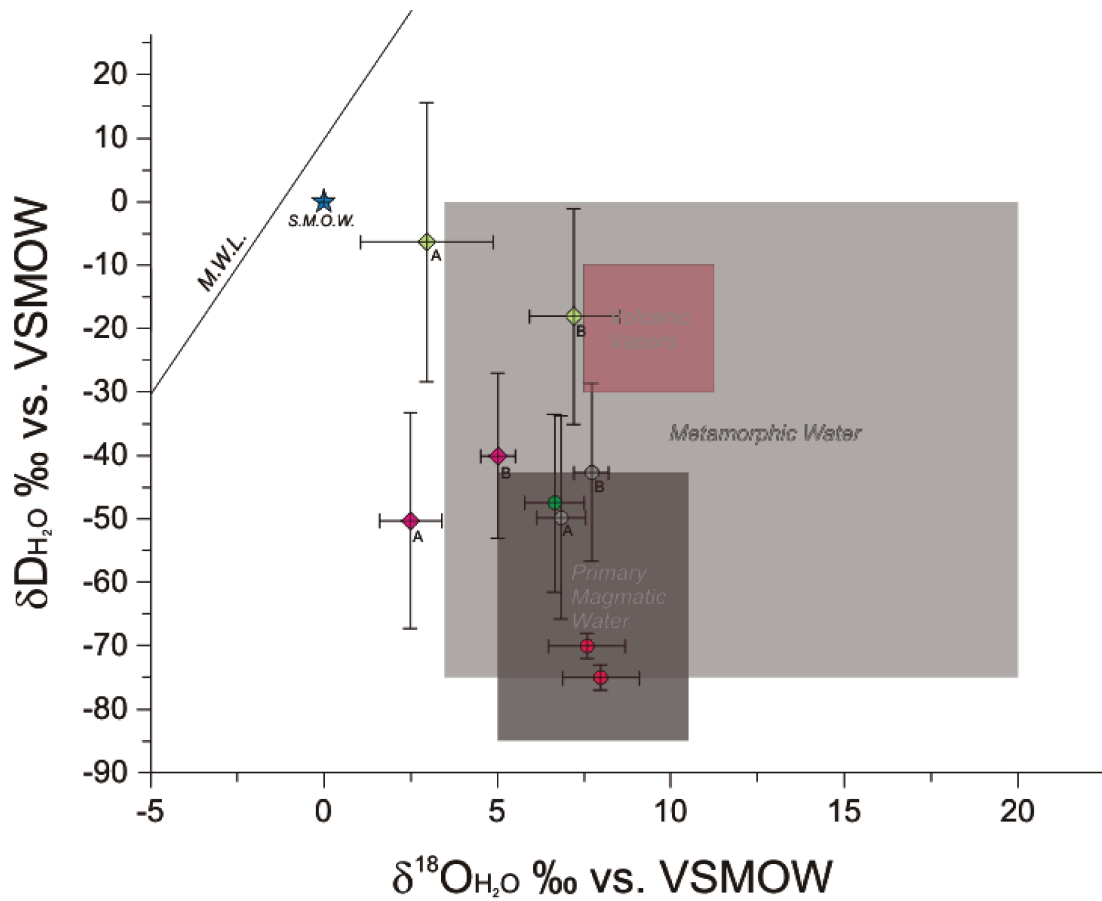
From **Tables 4** and **5**, the $\delta^{18}\text{O}_{\text{H}_2\text{O}}$ and $\delta\text{D}_{\text{H}_2\text{O}}$ values were calculated from isotopic data measured in hydrated minerals from both deposits (see **Table 6**) and these results are shown in **Figure 11** with special emphasis on different alteration stages.

For the calculation of $\delta^{13}\text{C}_{\text{fluid}}$ from calcite, we assumed that carbon was speciated as H_2CO_3 during ore formation and that H_2CO_3 isotopically behaves like CO_2 . The isotopic fractionation factor for carbon between calcite and CO_2 of Ohmoto and Rye (1979) was used to calculate the carbon isotopic composition of the fluid.

Table 6 – Calculated oxygen and hydrogen isotopic composition of fluids in equilibrium with hydrated minerals and associated error. Note: ^a – Almost all values were calculated using isotopic geothermometry, and it considers analytical error of 0.2‰ for oxygen and 2‰ for hydrogen. Values with * were calculated using empirical estimates of temperature, even though it considers analytical error. ^b – versus V-SMOW.

	Hydrothermal Alteration	Samples	$\delta^{18}\text{O}_{\text{H}_2\text{O}}$ (‰) ^{a,b}	Error $\delta^{18}\text{O}_{\text{H}_2\text{O}}$ (‰) ^{a,b}	$\delta\text{D}_{\text{H}_2\text{O}}$ (‰) ^{a,b}	Error $\delta\text{D}_{\text{H}_2\text{O}}$ (‰) ^{a,b}
Alvo Bacaba	Potassic Alteration (Biotite)	BACD03/41.46	2.5	0.9	- 50	17
		BAC25/341.25*	5.0*	0.5*	- 40*	13*
	Sericitization	BAC25/211.8*	7.2*	1.3*	-18*	17*
		BACD03/210	2.9	1.9	- 6	22

	Hydrothermal Alteration	Samples	$\delta^{18}\text{O}_{\text{H}_2\text{O}}$ (‰) ^{a,b}	Error $\delta^{18}\text{O}_{\text{H}_2\text{O}}$ (‰) ^{a,b}	$\delta\text{D}_{\text{H}_2\text{O}}$ (‰) ^{a,b}	Error $\delta\text{D}_{\text{H}_2\text{O}}$ (‰) ^{a,b}
Alvo Castanha	Sodic-calcic alteration /Magnetite formation	CTND02/358.16	8.0	1.1	- 75	2
		CTND02/368.7	7.6	1.1	- 75	2
	Potassic Alteration (Biotite)	CASD02/352	6.8	0.7	- 50	16
		CTND02/245.7	7.7	0.5	- 43	14
	Sericitization	CASD 01/69.9	6.6	0.9	- 47	14



Alvo Bacaba		Alvo Castanha	
◆	Biotite (A = 355 °C; B = 420 °C*)	●	Actinolite (350 °C)
◇	Sericite (A = 311 °C; B = 370 °C*)	●	Biotite (A = 376 °C; B = 422 °C)
		●	Sericite (446 °C)

Figure 10 – $\delta^{18}O$ versus δD plot from fluid in equilibrium with different hydrothermal alteration stages of the Alvo Bacaba and Alvo Castanha deposits, according to data from Table 3. Values for Magmatic Waters, Metamorphic Waters and Standard Mean Ocean Waters (SMOW) are from Sheppard (1986), for Volcanic Vapours are from Giggenbach (1992), and for the Meteoric Water Line (MWL) are from Craig (1967).

Estimated isotopic composition for fluids responsible for the pervasive sodic-calcic alteration, associated with actinolite and magnetite formation in the Alvo Castanha, corresponds to $\delta^{18}\text{O}_{\text{H}_2\text{O}} = 7.7 \pm 0.5\text{‰}$ and $\delta\text{D}_{\text{H}_2\text{O}} = -72 \pm 2\text{‰}$ at $345 \pm 25^\circ\text{C}$. The hydrothermal fluid associated with alkali feldspar from potassic alteration have $\delta^{18}\text{O}_{\text{H}_2\text{O}} = 6.2 \pm 1.0\text{‰}$ for the Alvo Bacaba and $\delta^{18}\text{O}_{\text{H}_2\text{O}} = 5.6 \pm 0.7\text{‰}$ for the Alvo Castanha deposit, at the temperature range of $450 \pm 50^\circ\text{C}$, which was taken to be close to that suggested for formation of feldspar-rich molecule orthoclase and anorthite-poor (500°C), formed in *subsolvus* conditions (Brown and Parsons 1989). Also, in the Alvo Castanha deposit, magnetite associated with alkali feldspar was formed from fluids with $\delta^{18}\text{O}_{\text{H}_2\text{O}} = 6.0 \pm 0.3\text{‰}$ at $450 \pm 50^\circ\text{C}$.

For the Alvo Bacaba deposit, the fluid in equilibrium with biotite and quartz, associated with the potassic alteration with biotite, has lower $\delta^{18}\text{O}_{\text{H}_2\text{O}}$ values ($5.1 \pm 0.3\text{‰}$) and $\delta\text{D}_{\text{H}_2\text{O}}$ of $-51 \pm 11\text{‰}$ at $420 \pm 10^\circ\text{C}$. Similar oxygen isotopic composition was estimated for chloritized biotite ($\delta^{18}\text{O}_{\text{H}_2\text{O}} = 5.1 \pm 0.3\text{‰}$), in the same temperature range.

In the Alvo Castanha, potassic alteration with biotite and quartz was developed from hydrothermal fluids with the estimated composition range: (Bt I) with lower values of $\delta^{18}\text{O}_{\text{H}_2\text{O}}$ ($7.5 \pm 0.4\text{‰}$) and $\delta\text{D}_{\text{H}_2\text{O}}$ ($-59 \pm 3\text{‰}$) at $440 \pm 20^\circ\text{C}$; and (Bt II) with slightly higher values of $\delta^{18}\text{O}_{\text{H}_2\text{O}}$ ($8.1 \pm 0.3\text{‰}$) and ($\delta\text{D}_{\text{H}_2\text{O}} = -54 \pm 2\text{‰}$) at $525 \pm 25^\circ\text{C}$.

For Alvo Bacaba, the fluid associated with sericite alteration, at $370 \pm 50^\circ\text{C}$, have two isotopic composition intervals; (SI) with $\delta^{18}\text{O}_{\text{H}_2\text{O}} = 3.4 \pm 1.4\text{‰}$, and (SII) with $\delta^{18}\text{O}_{\text{H}_2\text{O}} = 7.1 \pm 0.7\text{‰}$, with a similar hydrogen isotopic composition ($\delta\text{D}_{\text{H}_2\text{O}} = -17 \pm 8\text{‰}$) for both (SI) and (SII). In the Alvo Castanha, sericite alteration was developed at higher temperature from hydrothermal fluids with $\delta^{18}\text{O}_{\text{H}_2\text{O}} = 7.1 \pm 0.7\text{‰}$ at $500 \pm 50^\circ\text{C}$ (SIII); and $\delta^{18}\text{O}_{\text{H}_2\text{O}} = 8.7 \pm 0.3\text{‰}$ and $\delta\text{D}_{\text{H}_2\text{O}} = -55 \pm 2\text{‰}$ at $525 \pm 25^\circ\text{C}$ (SIV).

Carbonate alteration occurs associated with fluids with distinct isotopic composition in the two deposits. Higher $\delta^{13}\text{C}_{\text{fluid}}$ values have been reported only for the Alvo Castanha deposit. The **Figure 12** displays the estimated $\delta^{18}\text{O}$ versus $\delta^{13}\text{C}$ values for hydrothermal fluid associated with carbonate alteration from both Alvo Bacaba and Alvo Castanha deposits.

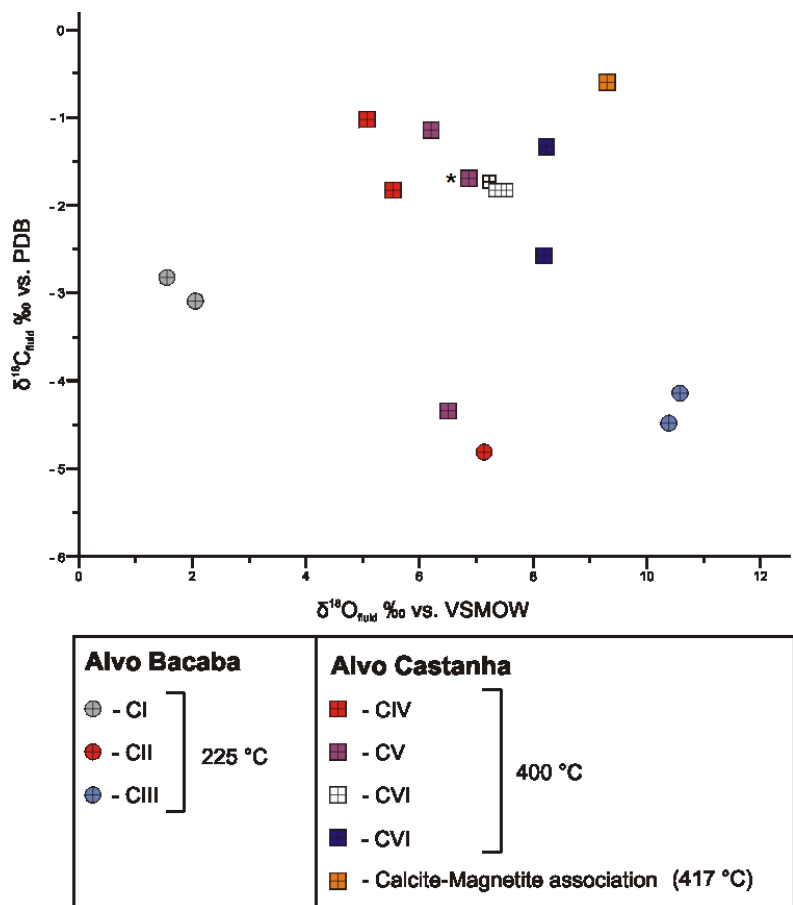


Figure 11 – $\delta^{18}\text{O}$ versus $\delta^{13}\text{C}$ graph of fluid in equilibrium with calcite. In the Alvo Bacaba, CI and CII associations correspond to the sampled calcite mineral associations (1) and (2), whereas CIII corresponds to the calcite association (3). In the Alvo Castanha all samples correspond to the association (4) with the exception of the association marked with (*), which corresponds to the association (5).

In the Alvo Bacaba, the carbonate alteration was related with fluids with (CI) $\delta^{18}\text{O}_{\text{H}_2\text{O}} = 1.8 \pm 0.5\text{‰}$ and $\delta^{13}\text{C}_{\text{H}_2\text{CO}_3} = -4.8 \pm 0.1\text{‰}$; (CII) $\delta^{18}\text{O}_{\text{H}_2\text{O}} = 7.1 \pm 0.2\text{‰}$ and $\delta^{13}\text{C}_{\text{H}_2\text{CO}_3} = -3.0 \pm 0.3\text{‰}$; (CIII) $\delta^{18}\text{O}_{\text{H}_2\text{O}} = 8.7 \pm 0.3\text{‰}$ and $\delta^{13}\text{C}_{\text{H}_2\text{CO}_3} = -4.3 \pm 0.3\text{‰}$, at a similar temperature range of $225 \pm 5^\circ\text{C}$. The association (CI) is characterized by apparent equilibrium between calcite and musketovite. Fluids in equilibrium with musketovite has $\delta^{18}\text{O}_{\text{H}_2\text{O}} = 1.7\text{‰}$ in the same temperature range.

On the other hand the Alvo Castanha, calcite formed from fluids, in an estimated temperature range of $400 \pm 50^\circ\text{C}$, with the following isotopic compositions: (CIV) $\delta^{18}\text{O}_{\text{H}_2\text{O}} = 5.2 \pm 1.0\text{‰}$ and $\delta^{13}\text{C}_{\text{H}_2\text{CO}_3} = -2.8 \pm 1.8\text{‰}$; (CV) $\delta^{18}\text{O}_{\text{H}_2\text{O}} = 6.3 \pm 1.1\text{‰}$ and $\delta^{13}\text{C}_{\text{H}_2\text{CO}_3} = -1.5 \pm 0.6\text{‰}$;

(CVI) $\delta^{18}\text{O}_{\text{H}_2\text{O}} = 7.3 \pm 1.0\text{‰}$ and $\delta^{13}\text{C}_{\text{H}_2\text{CO}_3} = -1.9 \pm 0.2\text{‰}$; (CVII) $\delta^{18}\text{O}_{\text{H}_2\text{O}} = 8.1 \pm 0.8\text{‰}$ and $\delta^{13}\text{C}_{\text{H}_2\text{CO}_3} = -2.0 \pm 0.8\text{‰}$. Calcite and magnetite formed from a fluid with $\delta^{18}\text{O}_{\text{H}_2\text{O}} = 9.5 \pm 0.5\text{‰}$ and $\delta^{13}\text{C}_{\text{H}_2\text{CO}_3} = -0.7 \pm 0.1\text{‰}$ at $417 \pm 12^\circ\text{C}$, although their textural equilibrium is not clear.

Associated hematite and musketovite (HI), selected in the Alvo Bacaba, formed from a fluid with estimated $\delta^{18}\text{O}_{\text{H}_2\text{O}} = 4.1 \pm 0.4\text{‰}$ at $90 \pm 10^\circ\text{C}$. Also in the Alvo Bacaba, hematite (HII) from calcite veins was in equilibrium with fluids with $\delta^{18}\text{O}_{\text{H}_2\text{O}} = 0.4 \pm 0.1\text{‰}$ at $190 \pm 40^\circ\text{C}$. For the Alvo Castanha, the estimated $\delta^{18}\text{O}_{\text{H}_2\text{O}}$ values ($6.6 \pm 0.3\text{‰}$) in equilibrium with magnetite from alkali feldspar veins is similar to that of fluids associated with magnetite-actinolite and magnetite-calcite.

Even though no quartz sample in textural equilibrium with sulfides have been observed, quartz from late veins with respect to the ore deposition or/and the previous alterations had its isotopic composition measured. The isotopic composition of the fluid associated with this late silicification was estimated based on temperature ranges calculated for quartz associated with sericitization and potassic alteration with biotite.

Quartz that fills open spaces in sulfide veins from Alvo Bacaba might have formed from a fluid with $\delta^{18}\text{O}_{\text{H}_2\text{O}} = 5.1 \pm 0.8\text{‰}$ at $415 \pm 45^\circ\text{C}$, which is similar to the isotopic composition of fluid in equilibrium with potassic alteration with biotite. In the same temperature range, late quartz veins from the Alvo Bacaba deposit, which crosscut pervasive potassic zones with biotite, display $\delta^{18}\text{O}_{\text{H}_2\text{O}} = 5.1 \pm 0.8\text{‰}$ identical to the value of quartz associated with sulfides. The **Figure 13** summarizes all estimates of fluid isotopic compositions described here.

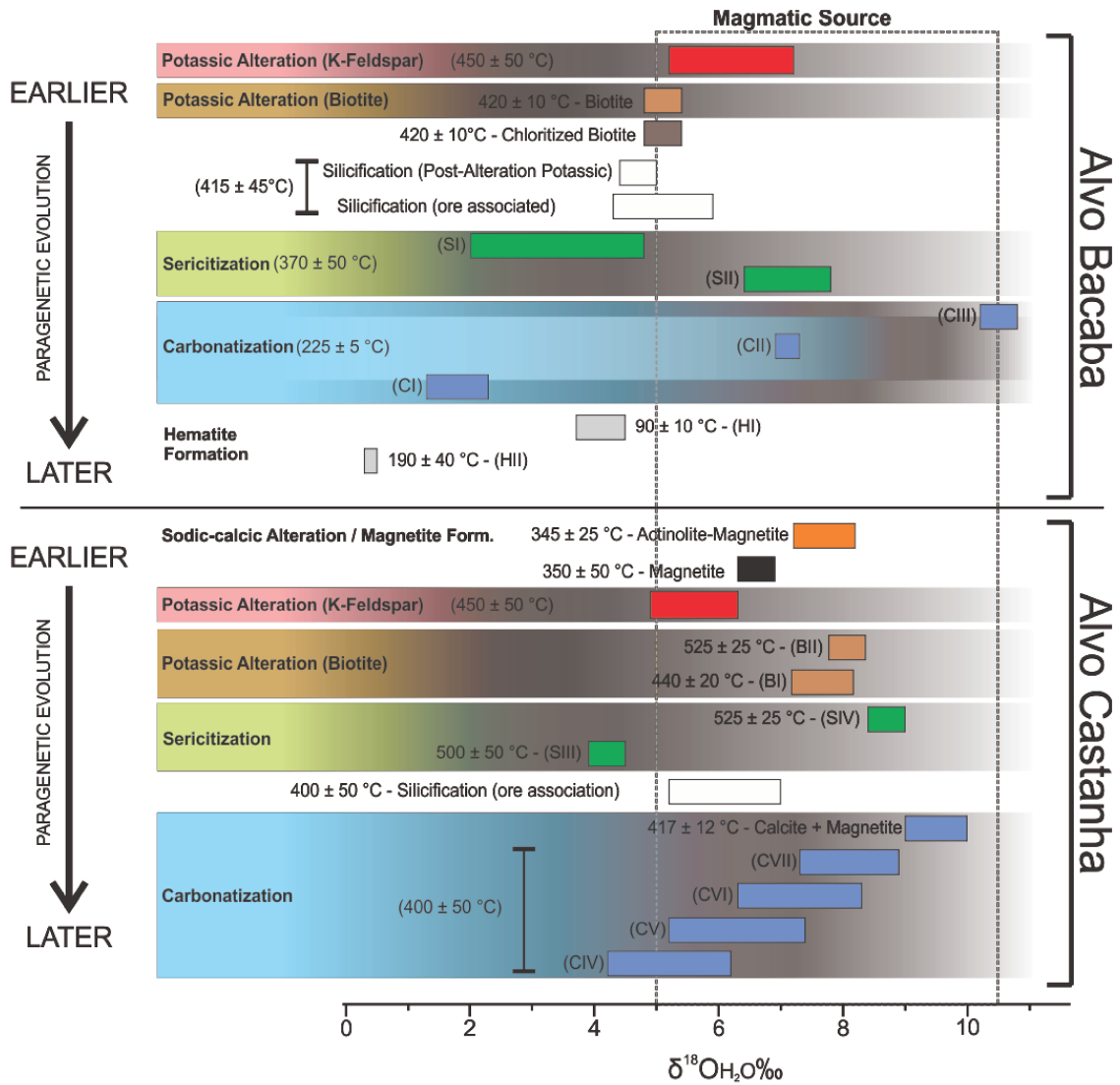


Figure 12 – Oxygen isotopic composition of hydrothermal fluids associated with different alteration stages and hydrothermal minerals from the Alvo Bacaba and Alvo Castanha deposits. Magmatic fluid values are from Sheppard (1986). Abbreviations according to **Table 5**.

6. SULFUR ISOTOPES

Sulfur isotopic analyses (**Figure 14**) were carried out on sulfides (chalcopyrite and pyrrhotite) associated with mineralized zones. The $\delta^{34}\text{S}_{\text{CDT}}$ values for the Alvo Bacaba deposit range from 1.3‰ to 5.4‰, while for Alvo Castanha vary from 0.1‰ to 3.0‰. Also chalcopyrite samples from other different copper deposits and occurrences of the Transition Domain were collected for comparison, including data from small irregular mines (1.2 to 1.5‰), Alvo Bacuri (0.8 to 1.1‰), Alvo Visconde (1.5‰), Pedra Branca and Alvo 118 deposits. **Figure 15** shows these values compared with those available in the literature.

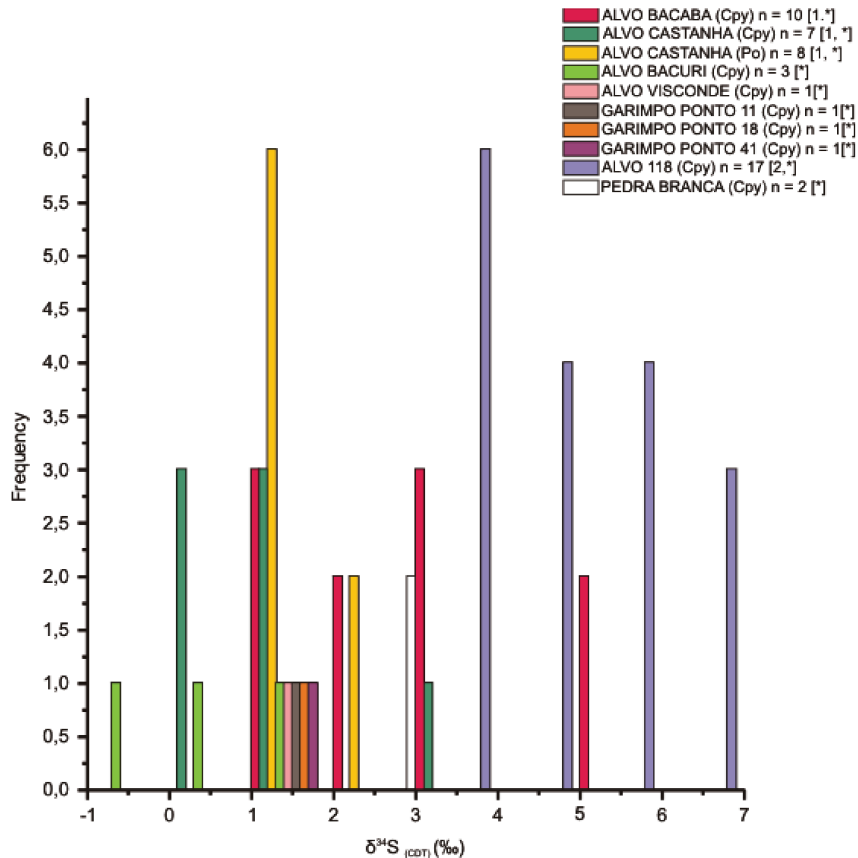


Figure 13 – $\delta^{34}\text{S}$ values for copper deposits (Alvo Castanha, Alvo Bacaba, Alvo Visconde, Alvo Bacuri and Pedra Branca) and small irregular mines (*garimpos*) in the Carajás Mineral Province. Note: * – This study; 1 – Monteiro *et al.* (2007); 2 – Torresi *et al.* (2009).

The $\delta^{34}\text{S}$ value for pyrrhotite sampled in Alvo Castanha directly reflects the fluid isotopic composition, because in redox and pH conditions of pyrrhotite precipitation all sulfur was

converted to H₂S (Ohmoto 1972). Also, as observed in all sampled deposits, without sulfates, the sulfur isotopic composition of sulfides is mainly equal from that of the sulfur source (Ohmoto 1972). Therefore the **Figure 15** shows that the major Cristalino deposit, the minor copper deposits (Alvo Castanha, Alvo Bacuri, Alvo Visconde, Pedra Branca), as well as the minor irregular mines (designated as Garimpo Ponto 11, Garimpo Ponto 18 and Garimpo Ponto 41) located near the Sossego Mine show sulfur isotopic composition strictly within the magmatic signature field. However, the Alvo Bacaba, Alvo 118, and the Sossego deposits show higher $\delta^{34}\text{S}$ values than those typical of magmatic source.

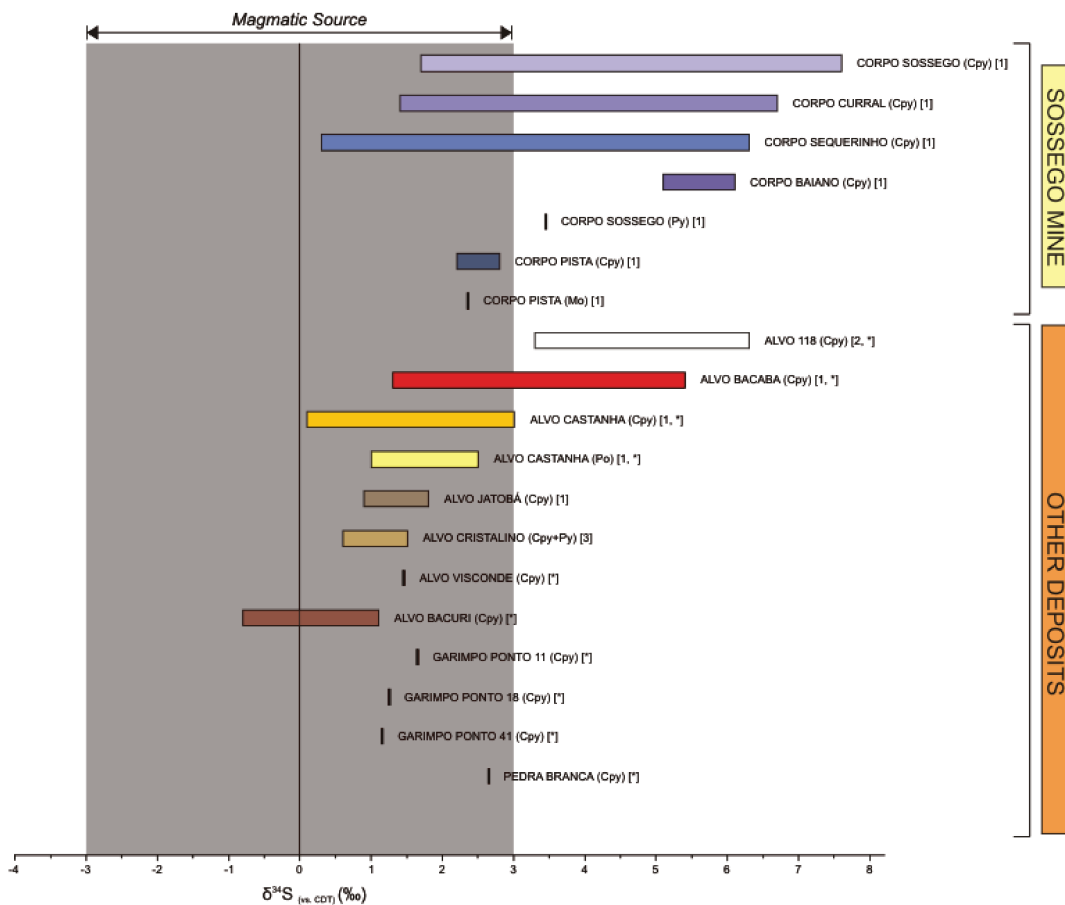


Figure 14 – Sulfur isotopic composition of sulfides from major iron-oxide-copper deposits at the Carajás Mineral Province (Sossego, Cristalino, Alvo 118), minor copper deposits (Alvo Castanha, Alvo Bacaba, Alvo Viconde, Alvo Bacuri and Pedra Branca), small irregular mines (*garimpos*). Note: * – This study; 1 – Monteiro *et al.* (2007); 2 – Torresi *et al.* (2009); 3 – Ribeiro (2008).

The spatial distribution of the highest values from all available data is displayed in an interpolated trend surface (**Figure 16**), which permits the regional view of the $\delta^{34}\text{S}_{\text{CDT-maximum}}$ variation among most deposits around the Sossego Mine. Considering the interpolation errors, it is clear that the higher $\delta^{34}\text{S}$ values are located close to the Sossego Mine, while lower $\delta^{34}\text{S}$ values occur in the eastern portion of Sossego and the minor copper deposits/occurrences.

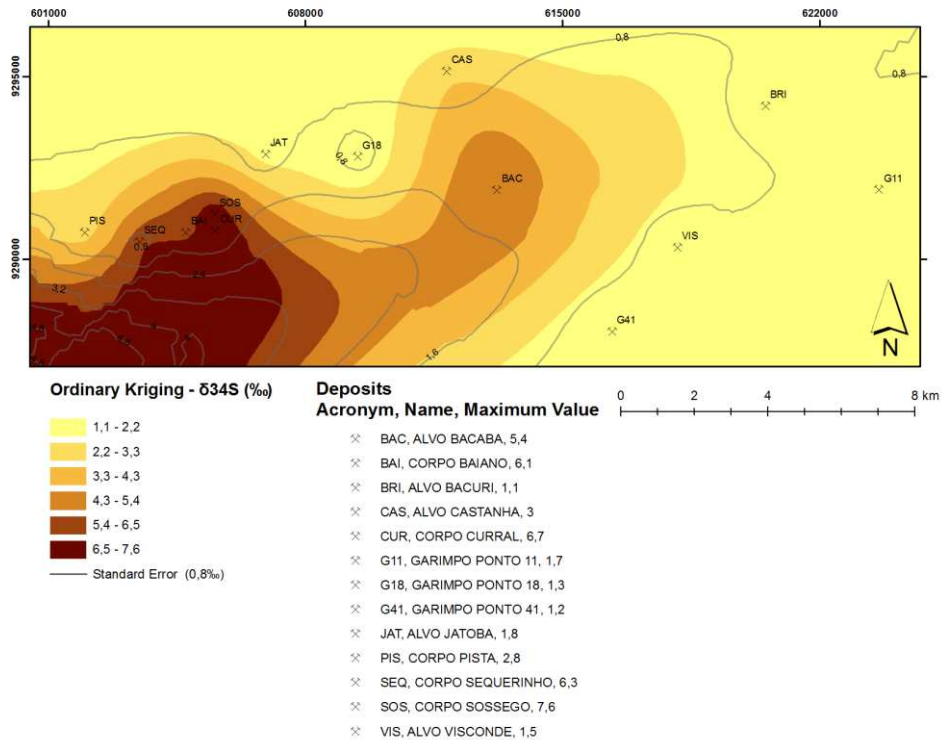


Figure 15 – Isovalue map for maximum $\delta^{34}\text{S}_{\text{CDT}}$ values for copper deposits on the surroundings of the Sossego Mine. The trend surface was obtained by ordinary kriging and the variogram was adjusted to the spherical model.

7. Discussion

7.1. HYDROTHERMAL SYSTEM EVOLUTION, FLUIDS AND SULFUR SOURCES

The Alvo Bacaba and Alvo Castanha deposits share a similar evolution indicated by the sequence of hydrothermal alteration stages accompanied by relative decrease of $\delta^{18}\text{O}$ values of the hydrothermal fluid and temperature. Nevertheless, according to mineral pair geothermometry and empirical estimations, the changes in temperature and $\delta^{18}\text{O}$ values were not the same for both deposits.

The Alvo Bacaba shows more abrupt decrease in temperature accompanying the paragenetic succession in relation to the Alvo Castanha deposit. Also, the Alvo Castanha, with few exceptions, displays higher $\delta^{18}\text{O}$ values of the hydrothermal fluid, and higher temperatures for the same hydrothermal alteration stages (*eg.* potassic alteration with biotite). Therefore the hydrothermal system in the Alvo Castanha area is marked by having evolved in conditions of higher temperature than the Alvo Bacaba.

Taking into account the paragenetic relationships in comparison to the temperature estimates (**Figure 13**) for the hydrothermal alteration stages, conditions for ore deposition may be inferred. The potassic alteration with biotite is earlier than the mineralization stage, whereas carbonatization is later in both deposits, suggesting that the mineralization stage in the Alvo Bacaba have occurred between 220 ° C and 410 ° C, while in the Alvo Castanha would have occurred between 350 ° C and 420 ° C.

Comparison of paragenetic evolution with the variation of $\delta^{18}\text{O}$ and δD values (**Figure 11 and Figure 13**) shows distinctive fluid isotopic signatures in the hydrothermal system. Oxygen and hydrogen isotopic data for the Alvo Bacaba deposit suggest that at least two fluid sources have contributed to the system: (i) a magmatic source with high $\delta^{18}\text{O}$ values; (ii) a non-magmatic source with low $\delta^{18}\text{O}$ values, which tends to be close to the Standard Mean Ocean Water composition, as noted in **Figure 11**. It might suggest: (1) a system that evolved through mixing of two fluids, one corresponding to water with composition near that of ocean water and another with magmatic signature; (2) a system that evolved from a non-magmatic fluid, with signatures of meteoric or low latitude oceanic waters, which acquired magmatic signature from assimilation through fluid-rock interaction with the igneous host rocks.

The $\delta^{18}\text{O}$ and δD values for the Alvo Castanha deposit are close to those of the magmatic water field (**Figure 11 and 13**) with a slight variation in the sericite and carbonate alteration

stages. It suggests a possible fluid contribution from non-magmatic sources depleted in heavy isotopes (eg. meteoric/ocean waters). Nevertheless, considering the inherent error for estimating the temperature by geothermometry, the high temperatures of the system and the predominance of isotopic composition within the field of primary magmatic water suggest for the Alvo Castanha deposit a genesis related to magmatic hydrothermal system.

The $\delta^{13}\text{C}$ values show that the mineralizing fluid from the Alvo Bacaba deposits was under conditions of oxygen fugacity ($f\text{O}_2$) greater than those of the Alvo Castanha, in accordance with the association of ore minerals of each deposit (pyrrhotite-chalcopyrite at Alvo Castanha) and (chalcopyrite-bornite at Alvo Bacaba).

The $\delta^{18}\text{O}$ versus $\delta^{13}\text{C}$ values (**Figure 12**) for carbonates from Alvo Bacaba indicate a small increase in the $f\text{O}_2$ during the hydrothermal system evolution, which is evidenced by a reduction in the $\delta^{13}\text{C}$ value of the hydrothermal fluid, and an increase in the $\delta^{18}\text{O}$ value possibly due to increased contribution of magmatic fluids. The $\delta^{13}\text{C}$ values of the Alvo Castanha hydrothermal fluid indicate lower oxygen fugacity than that of the Alvo Bacaba.

The sulfide $\delta^{34}\text{S}$ from both deposits show values near the composition of sulfur from magmatic source, but higher $\delta^{34}\text{S}$ values for the Alvo Bacaba sulfides could be caused by mixing of sulfur from different sources, such as sulfates from meteoric/ocean waters or, alternatively, from assimilation of sulfur from host rocks.

7.2. METALLOGENETIC IMPLICATIONS FOR THE SOSSEGO HYDROTHERMAL SYSTEM EVOLUTION

Geological and isotopic similarities among the Alvo Bacaba, Alvo Castanha and the Sossego orebodies might indicate that these deposits were formed in different portions of a single or similar hydrothermal systems.

From the standpoint of isotope geology, the evolution of the Alvo Bacaba, hosted by the 3.0 Ga Bacaba Tonalite and 2.86 Ga Serra Dourada Granite (Moreto *et al.*, 2011) is similar to that of the Sossego orebodies (Monteiro *et al.* 2008a). This evolution is characterized by a sudden reduction in temperature accompanied by decrease in $\delta^{18}\text{O}$ and increasing δD , which reflects a trend from a magmatic fluid signature to values close to those of ocean waters. The Alvo Castanha, which has predominance of nickel-enriched pyrrhotite-chalcopyrite breccias, however, shows magmatic sources for fluids, besides evidence of limited contribution from non-magmatic fluids.

The $\delta^{34}\text{S}$ values for Alvo Bacaba also show similarities with the Sossego orebodies (**Figure 15**), except to Corpo Pista (Monteiro *et al.* 2008a). However, the Alvo Castanha and other copper deposits (Alvo Bacuri, Alvo Visconde, Pedra Branca) and occurrences (*garimpos*) located westward from the Sossego Mine, displays mainly sulfur with magmatic signature. This might indicate a regional E-W trend (**Figures 16**) with regional prevalence of fluids with magmatic sulfur source and influx of external fluids with non-magmatic sulfur components along NE faults. This trend relates to the highest tonnages and metal content with higher $\delta^{34}\text{S}$ values, whereas the magmatic sulfur relates to the minor deposits with low metal content. The exception is the world-class Cristalino deposit, which could represent an example of major magmatic-dominant IOCG deposit.

However, a magmatic source for hydrothermal fluids is yet unknown, in part due to lack of robust geochronological data in the Carajás IOCG deposits. The available data are insufficient to connect a specific magmatic event with the genesis of the IOCG deposits (Monteiro *et al.* 2008a, Xavier *et al.* 2010). Because all host rocks from Sossego and other deposits in its vicinities are igneous, all interpretations converge to the following assumptions: (1) There were fluids from two distinct sources: non-magmatic and magmatic; (2) the hydrothermal fluids were essentially from non-magmatic source and assimilated the isotopic characteristics of igneous source through interaction with igneous host rocks.

Both hypotheses have been addressed in studies on boron isotopes, which indicated that some IOCG deposits in the Carajás Mineral Province, such as Salobo and Igarapé Bahia, have mostly boron from non-magmatic source, while the Corpo Pista orebody from the Sossego deposit displays boron contribution of a possible magmatic origin (Xavier *et al.* 2008). Additionally, studies of boron isotopes combined with systematic study of the Cl/Br-Na/Cl ratios, suggest that the fluids responsible for formation of these deposits, including Sossego, involved significant contribution of residual fluid from evaporative source (*eg.* brines generated by evaporation of sea water) that may have mixed with fluids of magmatic origin (Xavier *et al.* 2010).

Although controversial, due to the lack of geochronological data from ore genesis, the Alvo Castanha appears to be a magmatic end member, with a predominance of magmatic signature of oxygen, hydrogen, and sulfur. Also the Cl/Br-Na/Cl result obtained by R. P. Xavier (personal communication) for the Alvo Castanha points to a fluid of magmatic origin. Further, the Alvo

Bacaba data in comparison with data of the Sossego Mine (Monteiro *et al.*, 2008a; Xavier *et al.*, 2010) reinforce the evidence that there was a seawater contribution, or more specifically, ocean brines. This corroborates with the idea that Sossego IOCG deposits have originated from a magmatic-hydrothermal system in a marine paleoenvironment.

8. CONCLUSIONS

Despite the similarities of geological features, the Alvo Bacaba and Alvo Castanha deposits show distinct isotopic evolution of the hydrothermal systems. Both deposits have evolved with temperature decrease, but the temperature drop in relation to the hydrothermal alteration succession was greater in Alvo Bacaba than in the Alvo Castanha, and the oxygen fugacity was kept high at Alvo Bacaba during the process that culminated with ore deposition.

The ore deposition may have remained at similar temperature range, estimated for the Alvo Bacaba between 220 °C to 410 ° C, while the Alvo Castanha it would have occurred between 350 ° C and 420 ° C. The isotopic evolution of the Alvo Bacaba is similar to that of Sossego, with a steep temperature reduction accompanied by decrease of $\delta^{18}\text{O}$ and increase in δD values. This may suggest an evolving system with early fluids with magmatic isotopic signature that interacted with late fluids derived from ocean waters. This mixing process favors a broad range of sulfur composition from magmatic to non-magmatic sources. By contrast, the Alvo Castanha deposit appears to be an end member, with predominance of magmatic sources for both fluids and sulfur.

The correlation of these characteristics with those of Sossego strengthens the evidence that there was a contribution of magmatic and ocean waters in the hydrothermal system for the genesis of all these deposits.

ACKNOWLEDGEMENTS

The authors are grateful to VALE for allowing access to drill cores and providing logistical support to the UNICAMP researchers during field activities at Carajás. Special thanks are for Márcio Godoy, Benevides Aires and for all staff of the Sossego Mine who spent some valuable time helping us. We also would like to thank Professor Caetano Juliani and Carolina Penteadó Moreto for their help during drill core sampling and description and during regional geology fieldwork. This research has been supported by Conselho Nacional de Desenvolvimento Científico e Tecnológico (MCT/CNPq/CTMineral Project # 555065/2006-5) and Fundação de Amparo à Pesquisa do Estado de São Paulo–FAPESP (Procs. # 2009/02747-0).

REFERENCES

- Althoff FJ (1996) Etude pétrologique et structurale des granitöides de Marajoara (Pará, Brésil): leur rôle dans l'évolution archéenne du craton Amazonien (2.7 - 3.2 Ga). Université Henri Poincaré, Nancy I, Faculte des Sciences, Centre National de la Recherche Scientifique. Doctoral Thesis. 296p.
- Augusto RA, Monteiro LVS, Xavier RP, Souza Filho CR (2008) Zonas de Alteração Hidrotermal e Paragêneses do Minério Cuprífero do Alvo Bacaba, Província Mineral de Carajás. *Revista Brasileira de Geociências*, 38 (2): 263-277.
- Araújo OJB de, Maia RGN, Jorge João X da S, Costa JBS (1988). A megaestruturação arqueana da Folha Serra dos Carajás. In: VII Congresso Latino-Americano de Geologia – Anais. Belém, SBG-NO, 1: 324-338.
- Araújo OJB and Maia RGN (1991). Programa Levantamentos Geológicos Básicos do Brasil, Serra dos Carajás. Folha SB.22-Z-A. Estado do Pará. Escala 1:250.000. Brasília, DNPM/CPRM, 136p.
- Araújo OJB, Macambira EMB, Vale AG, Oliveira JR, Silva Neto CS, Costa EJS, Santos A, Pena Filho JIC, Neves AP, Jorge João XS, Costa JBS (1994). Primeira integração das investigações geológicas do Programa Grande Carajás na região SSE do Estado do Pará. In: SBG, Simp. Geol. Amaz., 4, Belém, Anais, p. 299-306.
- Avelar VG, Lafon JM, Correio JR, Macambira EMB (1999). O magmatismo Arqueano da região de Tucumã-Província Mineral de Carajás: novos resultados geocronológicos. *Rev. Bras. Geoc.* 29:454-460.
- Barros CEM, Macambira MJB, Barbey P, Scheller T (2004). Dados isotópicos Pb-Pb em zircão (evaporação) e Sm-Nd do Complexo Granítico Estrela, Província Mineral de Carajás, Brasil: Implicações Petrológicas e Tectônicas. *Bol. Museu Paraense Emilio Goeldi*, 34:531-538.
- Beisiegel VR, Bernardelli AL, Drumond NF, Ruff AW, Tremaine JW (1973). Geologia e recursos minerais da Serra dos Carajás. *Rev. Bras Geoc.*, 3:215-242.
- Bevington PR and Robinson DK (2002) Chapter 3: Error Analysis. In: *Data Reduction and Error Analysis for the Physical Sciences*, 3rd Ed., McGraw-Hill. p. 17-31.

- Brown WL and Parsosns I (1989) Alkali feldspars: ordering rates, phases transformation and behaviour diagrams for igneous rocks. *Min. Mag.* 53: 25-42.
- Carvalho ER, Xavier RP, Monteiro LVS, Souza Filho CR (2005) Geology and hydrothermal alteration of the Sossego iron oxide-copper-gold deposit, Carajás Mineral Province, Brazil. In: *Simpósio Brasileiro de Metalogenia*, 1, CD-ROM.
- Carvalho ER (2009) Caracterização geológica e gênese das mineralizações de óxido De Fe-Cu-Au e metais associados na Província Mineral de Carajás: estudo de caso do depósito de Sossego. Universidade Estadual de Campinas, Campinas, Brasil. Doctoral Thesis, 141 p.
- Cordeiro AAC (1999). Pesquisa mineral: panorama atual da CVRD. In: *VI Simpósio de Geologia da Amazônia*, p. 80-83.
- CPRM (2004) Carta Geológica do Brasil ao Milionésimo, Folha SB.22 – Araguaia 1:1.000.000.
- Costa JBS, Araújo OJB, Santos A, Jorge João XS, Macambira MJB, Lafon JM (1995). A província mineral de Carajás: aspectos tectono-estruturais, estratigráficos e geocronológicos. *Bol. Mus. Par. Emílio Goeldi – Série Ciências da Terra*, 7: 199-235.
- Craig H (1957) Isotopic standards of carbon and oxygen and correction factors for mass spectrometric analysis of carbon dioxide. *Geochim. Cosmochim. Acta* 12, 133– 149.
- Craig H (1967) Isotopic variations in meteoric waters. *Science*, 133:1702-1703.
- CPRM (2004) Carta Geológica do Brasil ao Milionésimo, Folha SB.22 – Araguaia 1:1.000.000.
- Dall’Agnol R, Lafon JM, Macambira MJB (1994) Proterozoic anaorogenic magmatism in the Central Amazonian Province, Amazonian Craton: geochronological, petrological and geochemical aspects. *Mineral Petrol.* 50: 113-118.
- Dias GS, Macambira MJB, Dall’Agnol R, Soares ADV, Barros CE (1996). Datação de zircões de sill de metagabro: comprovação da idade arqueana da Formação Águas Claras, Carajás - Pará. In: *SBG, Simpósio de Geologia da Amazônia*, 5, Extended Abstracts, p. 376-378.
- DOCEGEO - Rio Doce Geologia e Mineração S.A. (1988) Revisão litoestratigráfica da Província Mineral de Carajás – litoestratigrafia e principais depósitos minerais. *Congresso Brasileiro de Geologia*, 35, Belém, SBG, Anexo aos anais, p. 11-54.
- Feio GRL, Dall’Agnol R, Soares JEB, Gomes ACB (2009) Geoquímica do magmatismo granitóide arqueano da Região de Canaã dos Carajás. *XI Simp. Geol. Amazon.*, Manaus, CD-ROM.

- Galarza MA and Macambira MJB (2002) Geocronologia e evolução crustal da área do depósito de Cu-Au Gameleira, Província Mineral de Carajás (Pará), Brasil. *Geol. USP Série Científica*, 2: 143-159.
- Gomes ACB (2003) Geologia, petrografia e geoquímica dos granitóides de Canaã dos Carajás, SE do Estado do Pará. Belém, Centro de Geociências, Universidade Federal do Pará, Master Dissertation, 164 p.
- Gomes ACB and Dall’Agnol R (2007). Nova associação tonalítica-trondhjemítica neoarqueana na região de Canaã dos Carajás: TTGS com altos conteúdos de Ti, Zr e Y. *Rev. Bras. Geoc.*, 37(1): 182-193.
- Giggenbach WF (1992) Isotopic shifts in waters from geochemical and volcanic systems along convergent plate boundaries. *Earth and Planet. Sci. Lett.* 113: 495- 510.
- Graham CM, Harmon RS, Sheppard SMF (1984) Experimental hydrogen isotope studies: hydrogen isotope exchange between amphibole and water. *Am. Mineral.*, 69:128-138.
- Grainger CJ, Groves DI, Tallarico FHB, Fletcher IR (2008) Metallogenesis of the Carajás Mineral Province, southern Amazon Craton, Brazil: Varying styles of Archean through Paleoproterozoic to Neoproterozoic base- and precious-metal mineralization. *Ore Geol Rev* (in press doi:10.1016/j.oregeorev.2006.10.010).
- Hirata WK, Rigon JC, Kadokaru K, Cordeiro AAC, Meireles EA (1982) Geologia Regional da Província Mineral de Carajás. *Simp. Geol. Amaz.*, 1, Belém, 1982 Anais Belém, SBG/NO, v 1, p. 100-110.
- Hitzman MW (2000) Iron oxide–Cu–Au deposits: what, where, when, and why. In: Porter TM (ed) *Hydrothermal iron oxide copper–gold and related deposits: a global perspective* Austral Miner Fund, Adelaide, p. 9-25.
- Hitzman MW, Oreskes N, Einaudi MT (1992) Geological characteristics and tectonic setting of Proterozoic iron oxide (Cu-U-Au-REE) deposits. *Precambrian Res.* 58:241-287.
- Holdsworth R, Pinheiro R (2000) The anatomy of shallow-crustal transpressional structures: insights from the Archean Carajás’ fault zone, Amazon, Brazil. *J. Struct. Geol.* 22:1105-1123.
- Huhn SRB, Santos ABS, Amaral AF, Ledsham EJ, Gougêa JL, Martins LP, Montalvão RGM Costa VG (1988) O terreno “granito greenstone” da região de Rio Maria—Sul do Pará. XXXV Congresso Brasileiro de Geologia, vol. 3, p. 1438-1452.

- Huhn SRB and Nascimento JAS (1997) São os depósitos cupríferos de Carajás do tipo Cu-Au-U-ETR? In: Costa ML, Angélica RS (Coord.) Contribuições à Geologia da Amazônia. SBG, Belém, pp. 143-160.
- Huhn SRB, Souza CIJ, Albuquerque MC, Leal ED, Brustolin V (1999) Descoberta do depósito Cu(Au) Cristalino: Geologia e mineralização associada região da Serra do Rabo - Carajás – PA. SBG/NO, Simpósio de Geologia da Amazônia, 6, p. 140-143.
- Lancaster JA, Oliveira J, Fanton J, Almeida AJ, Leveille RA, Vieira S (2000) Discovery and Geology of the Sossego copper-gold deposit, Carajás District, Pará State, Brazil. In: VI Simpósio de Geologia da Amazônica, Abstracts, p. 48.
- Lindenmayer ZG (1990) Salobo sequence, Carajás, Brasil: Geology, Geochemistry and Metamorphism. Ph.D. thesis, University of Ontario, Canada, 407 p.
- Lindenmayer ZG, Teixeira, JBG (1999) Ore genesis at the Salobo Copper Deposit, Serra dos Carajás. In: Silva MG and Misi A (Eds.), Base Metal Deposits of Brazil. Belo Horizonte, MME/CPRM/DNPM, p. 33-43.
- Machado N, Lindenmayer Z, Krogh TH and Lindenmayer D (1991) U–Pb geochronology of Archaean magmatism and basement reactivation in the Carajás area, Amazon shield, Brazil. *Precamb. Res.*, 49: 329-354.
- McCrea JM (1950). On the isotopic chemistry of carbonates and a paleotemperature scale. *J. Phys. Chem.*, 18: 849-857.
- Monteiro LVS, Xavier RP, Souza Filho CR, Augusto RA (2007). Aplicação de isótopos estáveis ao estudo dos padrões de distribuição das zonas de alteração hidrotermal associados ao sistema de óxido de ferro-cobre-ouro Sossego, Província Mineral de Carajás. In: XI Congresso Brasileiro de Geoquímica, 2007, Atibaia. Anais. SBGq, CD-ROM.
- Monteiro LVS, Xavier RP, Carvalho ER, Hitzman MW, Johnson CA, Souza Filho CR, Torresi I (2008a) Spatial and temporal zoning of hydrothermal alteration and mineralization in the Sossego iron oxide–copper–gold deposit, Carajás Mineral Province, Brazil: parageneses and stable isotope constraints. *Miner. Depos.*, 43: 129-159.
- Monteiro LVS, Xavier RP, Hitzman MW, Juliani C, Souza Filho CR, Carvalho ER (2008b) Mineral chemistry of ore and hydrothermal alteration at the Sossego iron oxide copper gold deposit, Carajás Mineral Province, Brazil. *Ore Geology Reviews*, 34:3 317-336 (doi:10.1016/j.oregeorev.2008.01.003).

- Moreto CPN, Monteiro LVS, Xavier RP, Amaral WS, Santos TJS, Juliani C, Souza Filho CR (2011). Mesoarchean (3.0 and 2.86 Ga) host rocks of the iron oxide–Cu–Au Bacaba deposit, Carajás Mineral Province: U–Pb geochronology and metallogenetic implications. *Mineralium Deposita*. Online First, DOI: 10.1007/s00126-011-0352-9.
- Mougeot R, Respaut JP, Ledru P, Milesi JP, Macambira MJB and Huhn SB (1996). Contrainte géochronologique U-Pb pour l'âge de la formation sédimentaire de Águas Claras (Province de Carajás, Etat de Pará.). In: BRGM, Réunion des Sciences de la Terre, 16, Orléans, 67 p.
- Neves MP, Villas RN, Toro MAG (2006) Datação e avaliação da fonte dos metais do depósito do Sossego, região de Carajás: evidências isotópicas de Pb e Sm-Nd. In: SBG, Congr. Bras. Geol., 43, Anais, CD-ROM.
- Nogueira ACR, Truckenbrodt W, Pinheiro RVL (1995) Formação Águas Claras, Pré-Cambriano da Serra dos Carajás. Redescrição e redefinição o. *Boletim do Museu Paraense Emílio Goeldi. Série Ciências da Terra*, 7: 177-197.
- Ohmoto H (1972) Systematics of Sulfur and Carbon Isotopes in Hydrothermal Ore Deposit. *Economic Geology*, 67: 551-578.
- Ohmoto H (1986) Stable Isotope Geochemistry of Ore Deposits. In: Valley JW, Taylor HP JR, O'neil (eds.) *Stable Isotopes in High Temperature Geological Processes*, Mineralogical Society of America, *Reviews in Mineralogy*, v. 16, p. 491-560.
- Ohmoto H and Rye RO (1979) Isotopes of sulfur and carbon. In: Barnes HL (eds.) *Geochemistry of hydrothermal ore deposits*, 2nd, John Wiley and Sons, New York, p. 509 - 567.
- Oliveira MA, Dall'Agnol R, Althoff FJ, Silva Leite AA (2009) Mesoarchean sanukitoid rocks of the Rio Maria Granite-Greenstone Terrane, Amazonian craton, Brazil. *Journal of South American Earth Sciences*, 27: 146-160.
- Pestilho ALS and Monteiro LVS (2008) Caracterização petrográfica das zonas de alteração hidrotermal e paragêneses do minério de cobre e ouro do Alvo Castanha, Província Mineral de Carajás. *Simpósio de vulcanismo e Ambientes Associados*, 4, Foz do Iguaçu, CD-ROM.
- Pidgeon RT, Macambira MJB and Lafon JM (2000) Th–U–Pb isotopic systems and internal structures of complex zircons from an enderbite from the Pium Complex, Carajás Province, Brazil: evidence for the ages of granulite facies metamorphism and the protolith of the enderbite. *Chem. Geol.*, 166: 159-171.

- Pimentel MM, Lindenmayer ZG, Laux JH, Armstrong R, Araújo JC (2003) Geochronology and Nd geochemistry of the Gameleira Cu–Au deposit, Serra dos Carajás, Brazil: 1.8–1.7 Ga hydrothermal alteration and mineralization. *J. South Am. Earth. Sci.*, 15:803-813.
- Pinheiro RVL and Holdsworth RE (1997) Reactivation of Archaean strike–slip fault systems, Amazon region, Brazil. *J. Geol. Soc. London*, 154: 99-103.
- Ribeiro AA (2008). Litogeoquímica e geologia isotópica estável (C, S, O) do Depósito Cuproaurífero do Alvo Cristalino Sul, Província Mineral de Carajás, Pará. Universidade Federal do Pará, Dissertação de Mestrado. 126 p.
- Robinson MJ and Kusakabe M (1975) Quantitative preparation of SO₂ for ³⁴S/³²S analysis from sulfides by combustion with cuprous oxide. *Anal. Chem.*, 47:1179-1181.
- Rodrigues ES, Lafon JM, Scheller T (1992) Geocronologia Pb–Pb da Província Mineral de Carajás: primeiros resultados. Congresso Brasileiro de Geologia, 37, São Paulo. SBG, Resumos expandidos 2, p. 183-184.
- Sardinha AS, Dall’Agnol R, Gomes ACB, Macambira MJB, Galarza MA (2004) Geocronologia Pb-Pb E U-Pb em zircão de granitóides arqueanos da região de Canaã dos Carajás, Província Mineral de Carajás. Congr. Brasileiro de Geologia, 42, SBG, Araxá, Atas, CD-ROM.
- Sardinha AS, Barros CEM and Krymysky R (2006) Geology, geochemistry and U–Pb geochronology of the Archean (2.74 Ga) Serra do Rabo granite stocks, Carajás Metallogenic Province, northern Brazil. *J. S. Am. Earth Sci.*, 20: 327-339.
- Sharp ZD (1990) A laser-based microanalytical method for the in situ determination of oxygen isotope ratios in silicates and oxides. *Geochim. Cosmochim. Acta*, 54: 1353-1357.
- Sharp ZD and Kirschner DL (1994) Quartz-calcite isotope geothermometry: A calibration based on natural isotopic variations; *Geochim. Cosmochim. Acta*, 58: 4491-4501.
- Sheppard SMF (1986) Characterization and isotopic variations in natural waters. In: Valley JW, Taylor Jr. HP, O’Neil J (eds.) *Stable Isotopes in High Temperature Geological Process - Reviews in Mineralogy*, vol. 16. Mineralogical society of America, Chelsea. p. 165-183.
- Sousa FDS (2007). Estudo da alteração hidrotermal, com ênfase no metassomatismo sódico, de rochas granitóides e máficas da região de Canaã de Carajás, Província Mineral de Carajás. Universidade Federal do Pará, Master Dissertation.

- Souza ZS, Medeiros H, Althoff FJ, Dall'Agnol R (1990) Geologia do terreno granito - "greenstone" Arqueano da região de Rio Maria, sudeste do Pará. In: 36° Congr. Bras. Geol, SBG, Natal. Anais, 6: 2913-2928.
- Souza ZS and Dall'Agnol R (1995) Geochemistry of metavolcanic rocks in the Archean greenstone belt of Identidade, SE Pará, Brazil. Anais da Academeia Brasileira de Ciências, 76: 217-233.
- Souza SRB, Macambira MJB, Sheller T (1996) Novos dados geocronológicos para os granitos deformados do Rio Itacaiúnas (Serra dos Carajás, PA); implicações estratigráficas. Proceedings of the Simpósio de Geologia da Amazônia, Belém, Brazil, p. 380-383.
- Souza LH and Vieira EAE (2000) Salobo 3 Alpha deposit: geology and mineralization. In: Porter, T. M., ed., Hydrothermal Iron Oxide Copper-Gold and Related Deposits A Global Perspective, 1: Adelaide, Australia, Australian Mineral Foundation, p. 213-224.
- Souza ZS, Protel A, Lafon JM, Althoff FJ, Pimentel MM, Dall'Agnol R, Oliveira CG (2001) Nd, Pb and isotopes in the Identidade Belt, na Archean greenstone belt of the Rio Maria region (Carajás Province, Brazil): implications for the Archean geodynamic evolution of the Amazonian Craton. Precam. Res., 109:293-315.
- Suzuoki T and Epstein S (1976) Hydrogen isotope fractionation between OH-bearing minerals and water. Geochim. Cosmochim. Acta, 40: 1229-1240.
- Tallarico FHB, Coimbra CR, Cravo Costa CH (2000) The Serra Leste sediment-hosted Au-(Pd-Pt) mineralization, Carajás Province. Revista Brasileira de Geociências, 30: 226-229.
- Tallarico FHB (2003) O Cinturão Cupro-Aurífero de Carajás, Brasil. Tese de Doutorado, Universidade Estadual de Campinas, São Paulo, Brazil, 12 p.
- Tallarico FHB, Figueiredo BR, Groves DI, Kositcin N, McNaughton NJ, Fletcher IR, Rego JL (2005) Geology and SHRIMP U-Pb geochronology of the Igarapé Bahia deposit, Carajás copper-gold belt, Brazil: an Archean (2.57 Ga) example of iron-oxideCu-Au-(U- REE) mineralization. Econ Geol 100:7-28.
- Tassinari CCG and Macambira MJB (2004) A evolução tectônica do Cráton Amazônico. In: O desvendar de um continente: a moderna geologia da América do Sul e o legado da obra de Fernando Flávio Marques de Almeida (V. Mantesso Neto, A. Bartorelli C.D.R. Carneiro and B.B.B. Neves, eds.). Beca, São Paulo, Brazil, p. 471-486.

- Tavaza E (1999) Mineralização de Au-Cu-(ETR-U) associada às brechas hidrotermais do depósito de Igarapé Bahia, província Mineral de Carajás, PA. Dissertação de Mestrado, Ouro Preto, Brazil, Universidade Federal de Ouro Preto. 81 p.
- Taylor BE (1987) Stable geochemistry of ore-forming fluids. In: Stable isotope geochemistry of low temperature fluids. Short Course, 13, Mineralogical Association of Canada. p. 337-452.
- Torresi I, Bortholoto DFA, Xavier RP, Monteiro LVS (2009) Hydrothermal alteration, fluid inclusions and stable isotopes systematics of the Alvo 118 Iron-Oxide-Copper-Gold Deposits, Carajás Mineral Province (Brazil): Implications for ore genesis. *Mineralium Deposita*.
- Trendall AF, Basei MAS, De Laeter JR, Nelson DR (1998) SHRIMP U-Pb constraints on the age of the Carajás Formation, Grão Pará Group, Amazon Craton. *J. South Am. Earth. Sci.*, 11:265–277.
- Villas RN and Santos MD (2001) Gold deposits of the Carajás Mineral Province: deposit types and metallogenesis. *Mineralium Deposita*, 36: 300-331.
- Villas RN, Lima LFO, Neves MP, Sousa FDS, Lamarão CN, Fanton J, Morais R (2005) Relações entre deformação, alteração hidrotermal e mineralização no depósito Cu-Au do Sossego, Província Mineral de Carajás. In: Simpósio Brasileiro de Metalogenia, 1, CD-ROM.
- Villas RN, Neves MP, Moura CV, Toro MAG, Aires B, Maurity C (2006) Estudos isotópicos (Pb, C e O) no depósito Cu-Au do Sossego, Província Mineral de Carajás. In: SBG/Núcleo Norte, Simpósio de Geologia da Amazônia, 9, Resumos, CD-ROM.
- Wirth KR, Gibbs AK, Olszewski WJ (1986) U-Pb ages of zircons from the Grão Pará Group and Serra dos Carajás granite, Pará, Brasil. *Rev Bras Geocienc*, 16:195-200.
- Xavier RP, Wiedenbeck M, Trumbull RB, Dreher AM, Monteiro LVS, Rhede D, Araújo CEG, Torresi I (2008) Tourmaline B-isotopes fingerprint marine evaporites as the source of high-salinity ore fluids in iron oxide-copper-gold deposits, Carajás Mineral Province (Brazil). *Geology*, 36(9):743-746.
- Xavier RP, Monteiro LVS, Souza Filho CR, Torresi I, Carvalho ER, Dreher AM, Wiedenbeck M, Trumbull RB, Pestilho ALS, Moreto CPN. (2010) The Iron Oxide Copper-Gold Deposits of the Carajás Mineral Province, Brazil: An Updated and Critical Review. In: Porter, T.M.. (Org.). *Hydrothermal Iron Oxide Copper-Gold and Related Deposits: A Global Perspective, Advances in the Understanding of IOCG Deposits*. Adelaide: PGC Publishing, v. 3, p. 1-2.

- Zheng YF (1991) Calculation of oxygen isotope fractionation in metal oxides. *Geochim. Cosmochim. Acta*, 55: 2299-2307.
- Zheng YF (1993a) Calculation of oxygen isotope fractionation in anhydrous silicate minerals. *Geochim. Cosmochim. Acta*, 57: 1079-1091.
- Zheng YF (1993b) Calculation of oxygen isotope fractionation in hydroxyl-bearing silicates. *Earth and Planet. Sci. Lett.*, 120: 247-263.
- Zheng YF (1994) Oxygen isotope fractionation in metal monoxides. *Mineral. Mag.* 58A: 1000-1001.